

Review

# Atomic-Level Functionalized Graphdiyne for Electrocatalysis Applications

Xiaodong Qian <sup>1</sup>, Yongshen Zheng <sup>1</sup>, Songhua Chen <sup>2,\*</sup> and Jialiang Xu <sup>1,\*</sup>

<sup>1</sup> School of Materials Science and Engineering, National Institute for Advanced Materials, Nankai University, Tongyan Road 38, Tianjin 300350, China; qianxiaodong1016@163.com (X.Q.); zhengyongshen@mail.nankai.edu.cn (Y.Z.)

<sup>2</sup> College of Chemistry and Material Science, Longyan University, Longyan 364012, Fujian, China

\* Correspondence: songhua@iccas.ac.cn (S.C.); jialiang.xu@nankai.edu.cn (J.X.); Tel.: +86-022-8535-8786 (J.X.)

Received: 30 June 2020; Accepted: 4 August 2020; Published: 13 August 2020



**Abstract:** Graphdiyne (GDY) is a two-dimensional (2D) electron-rich full-carbon planar material composed of  $sp^2$ - and  $sp$ -hybridized carbon atoms, which features highly conjugated structures, uniformly distributed pores, tunable electronic characteristics and high specific surface areas. The synthesis strategy of GDY by facile coupling reactions under mild conditions provides more convenience for the functional modification of GDY and offers opportunities for realizing the special preparation of GDY according to the desired structure and unique properties. These structural characteristics and excellent physical and chemical properties of GDY have attracted increasing attention in the field of electrocatalysis. Herein, the research progress in the synthesis of atomic-level functionalized GDYs and their electrocatalytic applications are summarized. Special attention was paid to the research progress of metal-atom-anchored and nonmetallic-atom-doped GDYs for applications in the oxygen reduction reaction (ORR), the oxygen evolution reaction (OER) and the hydrogen evolution reaction (HER) catalytic processes. In addition, several potential development prospects and challenges of these 2D highly conjugated electron-rich full-carbon materials in the field of electrocatalysis are presented.

**Keywords:** graphdiyne; metal-atom-anchored graphdiyne; nonmetallic-atom-doped graphdiyne; oxygen reduction reaction; oxygen evolution reaction; hydrogen evolution reaction

## 1. Introduction

With the over-consumption of global fossil fuels and the increasing environmental pollution, the development and utilization of sustainable and clean energy as substitutes for conventional energy is an important way to achieve green sustainable development, but remains challenging [1–4]. Electrochemical catalysis of energy conversion technologies including fuel cells and metal–air batteries has been extensively and intensively investigated for its key role in building sustainable development and environment-friendly energy cycles [5]. Different combinations of catalytic reactions have realized diverse energy storage and conversion systems, such as fuel cells (ORR/HOR), water splitting (OER/HER), metal–air batteries (ORR/OER) [6]. Unfortunately, owing to the very slow electrochemical reactions kinetics of the ORR and OER, their practical applications are greatly restricted [7–9]. To date, the noble-metal-based catalysts such as Pt and  $RuO_2$  have demonstrated their high catalytic activity in electrocatalysis [10,11] and have been therefore regarded as benchmark catalysts [12,13]. However, the high price and scarcity of these catalysts seriously hamper the development of their commercial applications. Thus, the development and utilization of electrocatalysts is of vital importance within its characteristics of efficiently promoting the slow kinetic process of ORR and OER while greatly improving the energy conversion efficiency. At the same time, it is essential to develop highly

efficient and stable HER catalysts that can replace Pt catalysts [14,15]. In these regards, the unique two-dimensional (2D) carbon material that has two value features of a tunable and uniformly exposed crystal-plane and a unique electronic structure has attracted people's attention [16,17]. In particular, its atomic thickness and large surface area contributes to the exposure of a large number of active sites and the fast transport of carrier [18–21], and its huge advantages of high energy conversion efficiency and environmental friendliness have promised their applications in the field of electrocatalysis [22–25].

Graphdiyne (GDY) has emerged as the new generation of 2D nanostructured carbon material containing  $sp^2$ - and  $sp$ -hybridized carbon atoms, with high degrees of  $\pi$  conjugation, natural uniform porous structure, superior semiconducting properties and excellent chemical and mechanical stability [26–30]. The  $sp^2$ - and  $sp$ -hybridized acetylene bonds and benzene rings constitute the single-atomic layer 2D GDY (Figure 1a). Similar to graphene, in the infinite planar extension, the single-layer 2D planar configuration of GDY will form certain folds in order to maintain the stability of the configuration (Figure 1b) [31]. Due to its unique conjugated electronic structure [32], extraordinary conductivity and adjustable electronic characteristics [33,34], GDY with controllable full-carbon framework of atomic thickness has been applied in the field of electrocatalysis [35–39]. In the structure of GDY, adjacent benzene rings ( $sp^2$ -hybridized carbon) linked to each other through butadiyne linkages ( $sp$ -hybridized carbon) [40]. Furthermore, in addition to  $sp^2$  hybridization, the  $sp$  hybridization makes the arbitrary angle rotation of  $\pi/\pi^*$  perpendicular to the axis, which sorts the possibility of pointing toward atoms and coordinating with atoms [41]. Another important advantage that GDY can grow in situ on arbitrary substrate [42,43] provides better basic conditions for its manufacture of stable catalysts and efficient catalytic effects. Thereby, GDY is rapidly becoming a valuable member of 2D all-carbon conjugated material system and contributing to the commercial and industrial development in the field of electrocatalysis.

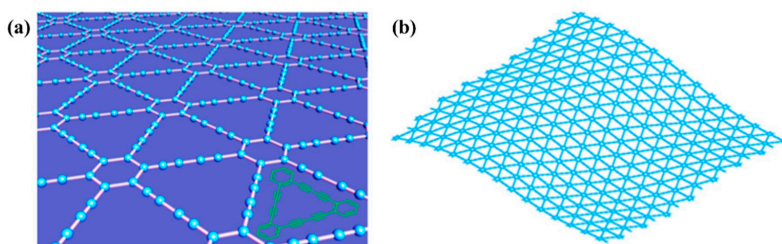


**Figure 1.** Chemical structure of GDY [31]. (a) Schematic diagram of the two-dimensional planar configuration of the single atomic layer of GDY. (b) Schematic diagram of the folds of the two-dimensional planar configuration of GDY.

In this review, we summarize the recent progress on the synthesis of atomic-level functionalized GDY catalysts and their electrocatalysis applications. The atomic-level functionalization of GDY is divided into two parts, namely the metal-atom-anchored functionalized GDY catalysts and the nonmetallic-atom-doped functionalized GDY catalysts. Their applications in the field of electrocatalysis will cover three aspects of ORR, OER and HER catalysis, which are discussed from both theoretical predictions and experimental investigations. This study briefly looks ahead to the challenges and opportunities in the future of attempting to fully and efficiently utilize the full advantages of GDY to construct the electrocatalysts with commercial application value.

## 2. Synthesis of Atomic-Level Functionalized GDY Catalysts

In addition to the copper foil method to synthesize GDY (Figure 2a), the chemical vapor deposition (CVD) (Figure 2b–c) [44], the gas/liquid interface method (Figure 2d) and liquid/liquid interface method (Figure 2e) [27] have also been demonstrated to be feasible for the synthesis of GDY. Large-scale and various forms of (nanofilms [27], ultrathin nanosheets [19,45], nanowalls [46], nanotubes [47] and nanochains [48]) of high quality GDY can be feasibly prepared in the required form. These GDY samples with various morphologies are prerequisites for achieving high-performance nonmetallic

catalyst or metal catalyst support. Simultaneously, on account of the closed environment formed in the interface method contributing to the excellent continuity and superior 2D features of the as-prepared GDY [49,50], this high-quality 2D structure is the most necessary condition for the realization of GDY-based materials as electrocatalysts. More important, GDY has been predicted to be the most stable carbon network containing diacetylenic bonds, and the existence of acetylenic bonds offer innovative methods for structural flexibility along with property modification, making it favorable for wider applications compared with conventional 2D materials [51,52]. Overall, GDY is highly controlled in synthesis in terms of its structure and physicochemical properties together with the uniformly distributed cavities, which promises the possibility to achieve the desired physical and chemical properties through the functionalization at atomic-level [53].

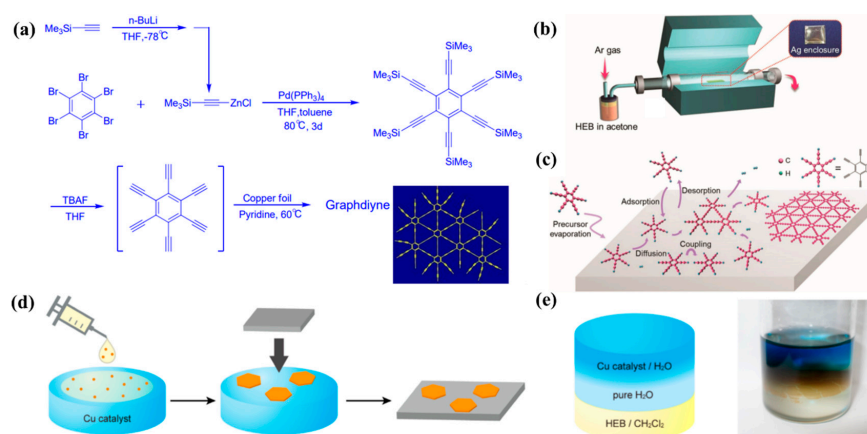


**Figure 2.** Syntheses of GDY. (a) Synthetic route of GDY film by copper foil method (reproduced with permission from [26]. Copyright The Royal Society of Chemistry, 2010); (b) experimental setup of the chemical vapor deposition (CVD) system for the growth of GDY on silver surface using hexaethynylbenzene (HEB) as precursor; (c) schematic view of the surface growth process by CVD method (reproduced with permission from [44]. Copyright Wiley-VCH, 2017); (d) schematic illustration of the gas/liquid interfacial synthesis and transfer process. A very small amount of HEB (20 nmol) in a mixture of dichloromethane and toluene (220  $\mu$ L, 1:10 *v/v*) was gently placed on the surface of an aqueous solution containing the copper catalyst at room temperature under Ar atmosphere. Catalytic polymerization proceeded at the gas/water interface for 24 h, producing a GDY nanosheets that floated on the interface. The GDY nanosheets can be transferred onto various flat substrates via a horizontal approach known as the Langmuir–Schaefer method; (e) schematic illustration and a photograph of the liquid–liquid interfacial synthetic procedure. Under Ar atmosphere at room temperature, the successive catalytic coupling reaction for 24 h led to the growth of the 2D covalent network, generating a multilayer GDY film at the liquid/liquid interface (reproduced with permission from [27]. Copyright American Chemical Society, 2017).

### 2.1. Synthesis of Metal-Atom-Anchored GDY Catalysts

The metal-atom catalysts have aroused great interest owing to the characteristics of exposing the maximum number of active sites, maximizing the utilization of metal atoms and having high efficiency and stable catalytic performance, consisting of single metal atoms anchored on the supporting material [54–56]. Isolated metal atoms with high surface energy make them easy to agglomerate into metal nanoparticles and their thermodynamic instability also challenges the controllable preparation of stable metal-atom catalysts. Thus, it is vital to develop suitable synthetic methods to prepare metal-atom catalysts with highly dispersed metal atoms and stable performance. The three key points for preparing highly efficient, stable and durable metal-atom catalysts are as follows: (a) High physical and chemical stability and high surface area to stably and effectively anchor as many metal atoms as possible; (b) The effective distribution of metal atoms on the surface of the support to exert its maximum catalytic activity; (c) The strong interaction between the metal-atom and the support to ensure the overall

performance of the catalyst. Due to its advantages of high conjugated structure, large specific surface area and high adsorption energy for metal atoms, GDY is considered to be the excellent support for efficiently and stably anchoring metal atoms [57–60]. The formation of strong covalent bonds between metal atoms and carbon atoms in the GDY structure is a guarantee of their excellent electrocatalytic performance. Thus, far, the two main methods developed for preparing metal-atom catalysts supported by GDY are the wet chemical method and the electrochemical deposition method, respectively.

### 2.1.1. Wet Chemical Method

The wet chemical method for preparing metal-atom catalysts involves the addition of the support and metal precursor in the same solution and the distribution of the metal precursor on the support by wet impregnation, co-precipitation or deposition-precipitation. The metal is changed from oxidation state to zero or low valence state by reducing agent and finally a catalyst in which metal atoms are anchored on a support is obtained. Maintaining the suitable metal loading on the support surface is critical for the synthesis of metal-atom catalysts. High metal loadings may cause the aggregation of metal atoms together to form metal clusters or metal nanoparticles [61]. The primary principle of preparing the stable metal-atom catalysts is to enhance the interaction between metal atoms and the support while maintaining an appropriate metal loading on the support. Yin et al. [62] used  $K_2PtCl_4$  as the metal precursor and successfully anchored Pt single atom on the surface of GDY by in situ wet chemistry. No obvious Pt clusters or nanoparticles are formed. The white bright spots as shown in Figure 3a have diameters of about 1.9–2.3 Å, close to the theoretical atomic diameter of the Pt single atom. Notably, the sp-hybrid alkynyl carbon atom in the 18C-hexagonal holes in GDY framework is the ideal anchoring site for Pt atoms. It is confirmed that the Pt atoms are anchored by forming a coordinated interaction with C atoms on the alkynyl group, which further confirms that Pt is anchored on the surface of GDY in the form of isolated atoms.

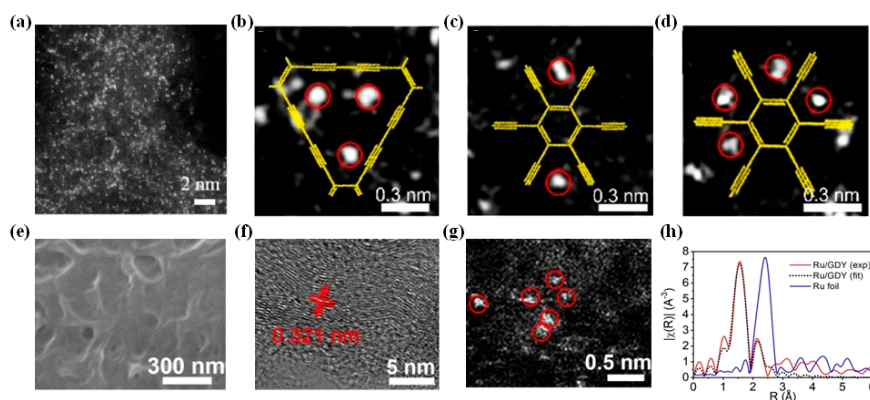


**Figure 3.** Structural characterizations of metal-atom-anchored GDY. (a) Atomic-resolution high-angle annular dark-field scanning transmission electron microscopy (HAADF-STEM) image for Pt-GDY (reproduced with permission from [62]. Copyright Wiley-VCH, 2018); (b–d) different configurations of the individual Mo-atoms anchored on the GDY structure (reproduced with permission from [63]. Copyright American Chemical Society, 2018); (e) scanning electron microscopy (SEM), (f) High-resolution transmission electron microscopy (HRTEM) and (g) HAADF images of Ru/GDY; (h) Experimental and fitted EXAFS spectra of Ru/GDY and Ru foil (reproduced with permission from [64]. Copyright Elsevier, 2020).

Using  $Na_2MoO_4$  as the metal precursor, Hui et al. [63] successfully anchored the Mo atom on the surface of GDY (Mo/GDY) through the solvothermal reduction wet chemistry method, with the average loading of metal Mo atoms of 7.5 wt%. The isolated and uniform bright points in the Figure 3b–d confirm the successful anchoring of Mo atoms and also display the local coordination environment of Mo atoms in the sample, providing evidences for possible anchor configurations of Mo metal atoms. By a facile and effective in-situ wet-chemical reduction strategy, ruthenium (Ru) atom was

easily anchored on the GDY grown on a 3D carbon fiber network, and the self-supporting 3D flexible GDY-supported Ru atom catalyst (Ru/GDY) with the 1.0 wt% loading of Ru atom was prepared [64]. The Ru/GDY sample has a well-defined 3D layered structure (Figure 3e) and the presence of Ru atoms can be observed (Figure 3f,g). It is worth noting that the stripe spacing of Ru/GDY (0.321 nm) is smaller than that of the original GDY (0.365 nm), indicating the existence of the interactions between the Ru atoms and the GDY. The extended X-ray absorption fine structure (EXAFS) spectrum of Ru/GDY (Figure 3h) features a predominant peak at 1.54 nm, which is smaller than that of the Ru–Ru contribution (at ~2.41 nm) in Ru foil. It is also noted that the adsorption edge of Ru/GDY shifts to higher energy position corresponding to RuO<sub>2</sub> [65,66] compared to Ru foil, reflecting the only presence of isolated Ru atoms in Ru/GDY with a valence of about +4.

### 2.1.2. Electrochemical-Deposition Method

The preparation of metal-atom-anchored GDY catalysts by electrochemical-deposition method uses the GDY support as the cathode of the electrolytic cell and the metal salt solution with an appropriate ion concentration as the electrolyte. By applying a suitable voltage, the metal ions in the solution obtain electrons at the cathode and are reduced to be deposited on the GDY support. The simple and feasible electrochemical-deposition method is widely used owing to its unique advantages. The quality and the size of the deposited metal can be precisely controlled by controlling parameters such as the concentration of the plating precursor and the plating time. At the same time, electroplating can maximize the use of metal because it mainly deposits metal atoms on the outermost surface of the support. Xue et al. [67] successfully prepared Ni/Fe metal-atom-anchored GDY catalysts by electrochemical-deposition method using NiSO<sub>4</sub>/FeCl<sub>3</sub> as the electrolyte at a current density of 10 mA cm<sup>-2</sup> (Figure 4a). The metal-atom loadings of Ni/GDY and Fe/GDY prepared by this method were 0.278 wt% and 0.680 wt%, respectively and the metal exists in the form of atoms while forming a covalent bond with C atom in the GDY framework (Figure 4b,c). Similarly, the Pd-metal atom anchored GDY catalyst (Pd-GDY) was prepared by electrochemical-deposition (current density: 2 mA cm<sup>-2</sup>, deposition time: 10 s) using the sulfuric acid solution of PdCl<sub>2</sub> as the electrolyte [68]. The EXAFS spectrum of Pd-GDY (Figure 4d) features a major peak near 1.5 Å, corresponding to Pd–C contribution without the appearance of the Pd–Pd contribution (2.5 Å), demonstrating the only presence of isolated metal Pd atoms. Furthermore, the first derivative of X-ray absorption near-edge structure (XANES) is used as the basis for energy calibration and determination of the valence state of the samples [69]. The main peaks of Pd/GDY and Pd foils located at the same energy position (Figure 4e), which is the evidence that Pd atoms are anchored on the surface of GDY in a zero-valence state.

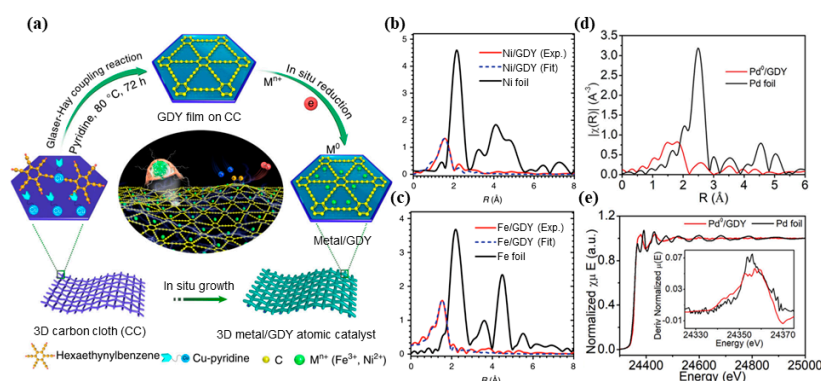


**Figure 4.** Synthesis and structural characterizations of metal-atom-anchored GDYs. (a) Schematic diagram of the synthetic route of Ni/GDY and Fe/GDY; (b) EXAFS spectra of Ni/GDY and Ni foil at the Ni K-edge; (c) EXAFS spectra of Fe/GDY and Fe foil at the Fe K-edge (reproduced with permission from [67]. Copyright Springer Nature, 2018); (d) EXAFS spectra of Pd<sup>0</sup>/GDY and Pd foil at the Pd K-edge; (e) normalized Pd K-edge XANES spectra and first-derivative curves (the inset) of Pd<sup>0</sup>/GDY and Pd foil (reproduced with permission from [68]. Copyright Elsevier, 2018).

## 2.2. Synthesis of Nonmetallic-Atom-Doped GDY Catalysts

Nonmetallic-atom doping is regarded as one of the important ways to adjust the properties of materials [70,71]. For example, some synthesis methods have been applied to directly prepare nitrogen-doped graphene, such as chemical vapor deposition (CVD) [72], segregation growth [73], solvothermal [74] and arc-discharge approaches [75]. Until now, the exploration of the synthesis method of nonmetallic-atom-doped GDY catalysts is not so comprehensive. The high-temperature annealing method, a traditional method for the heteroatom doping on carbon materials [76], has been used as the main synthesis method. By means of reasonable planning and utilization of high-temperature, the nonmetallic-atoms doped, or multi-atom co-doped GDY catalysts were also successfully synthesized. Yang et al. prepared a sulfur (S) atom-doped GDY (S-GDY) catalyst by a simple thermal synthesis procedure (Figure 5a) using short S radicals, generated through the homolysis of benzyl disulfide (as the S source) that can be bonded to the acetylenic bonds [77]. In another exploration, Zhao et al. used melamine and dibenzyl sulfide as continuous doping sources and successfully prepared N and S atom co-doped few-layer GDY catalyst by an improved pyrolysis method [78]. Likewise, GDY was calcined with thiourea, boron oxide and ammonium fluoride at 700 °C under Ar atmosphere to obtain single atom-doped GDY (SGDY, BGDY and FGDY), calcined under NH<sub>3</sub> atmosphere to obtain GDY co-doped with multiple-atoms (NSGDY, NBGDY and NFGDY) (Figure 5b) [79].

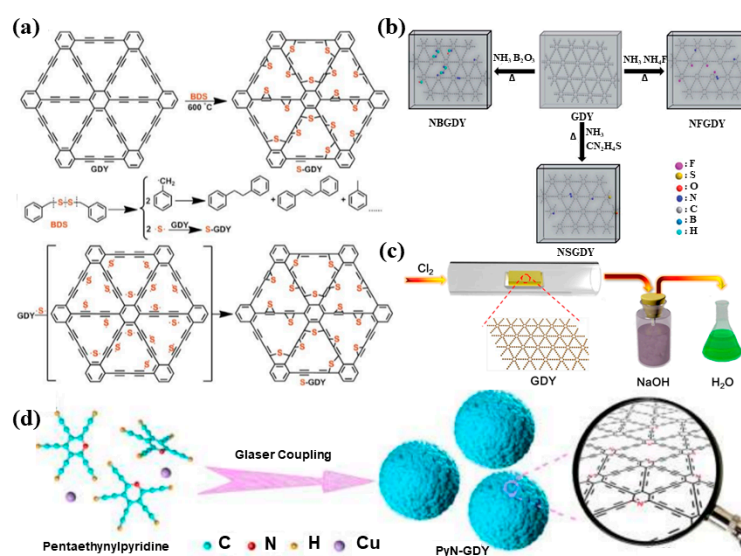


**Figure 5.** Syntheses of nonmetallic-atom-doped GDY. (a) Schematic illustration of the preparation of S-GDY (reproduced with permission from [77]. Copyright Wiley-VCH, 2019); (b) schematic drawing for the fabrication of multi-element-doped-GDY-based materials (reproduced with permission from [79]. Copyright The Royal Society of Chemistry, 2016); (c) schematic illustration of the preparation process of Cl-GDY (reproduced with permission from [80]. Copyright American Chemical Society, 2019); (d) Schematic illustration of the synthetic route of PyN-GDY (reproduced with permission from [81]. Copyright Elsevier, 2019).

Except the high-temperature annealing method, other direct and effective methods have been also developed for the synthesis of nonmetallic-atom-doped GDY catalysts. Firstly, a corrosion engineering strategy was applied to prepare ultrathin Cl-doped GDY (Cl-GDY) [80]. The pristine GDY prepared by the Glaser–Hay coupling reaction with hexaethynylbenzene (HEB) as the monomer in pyridine solution was put into a home-built tube furnace system for annealing with Ar as a carrier gas and Cl<sub>2</sub> gas as the chlorine source and etching gas to prepare Cl-doped GDY catalyst (Figure 5c). Secondly, by using the bottom-up synthesis strategy as the guiding ideology, the GDY catalyst with a specific configuration of nitrogen selective doping was prepared by using a Glaser–Hay coupling reaction with pentaethynylpyridine as the monomer, in which one carbon atom in every benzene ring of

GDY is substituted by pyridine N (PyN-GDY) (Figure 5d) [81]. Third, in order to precisely adjust the ratio of doping atoms and the doping sites to control the variables in the experimental study, Zhao et al. introduced a new form of N-doping moieties (sp-N atoms) in the 2D layered GDY through the pericyclic reaction and successfully prepared sp-N-doped few-layer GDY catalysts [82].

With the high-temperature annealing method, the preparation of nitrogen (N) atom-doped GDY catalyst was achieved by heating GDY in a mixed atmosphere of high purity ammonia and argon [83]. The doping of N atoms changes the sample powder from the original relatively regular laminar morphology (Figure 6a) to the three-dimensional aggregation morphology of spherical particles (Figure 6b), but still maintains the amorphous structure (Figure 6c,d). Meanwhile, compared with GDY composed of C and physically adsorbed O from air, the appearance of both N 1s peak and C=N- in-N-doped GDY (N-GDY) indicates the successful doping of N atoms into the GDY network (Figure 6e,g). The N atoms have two bonding characters in the GDY network, corresponding to the imine N (N substitution of the sp-hybridized carbon atoms) and the pyridinic N (Figure 6h).

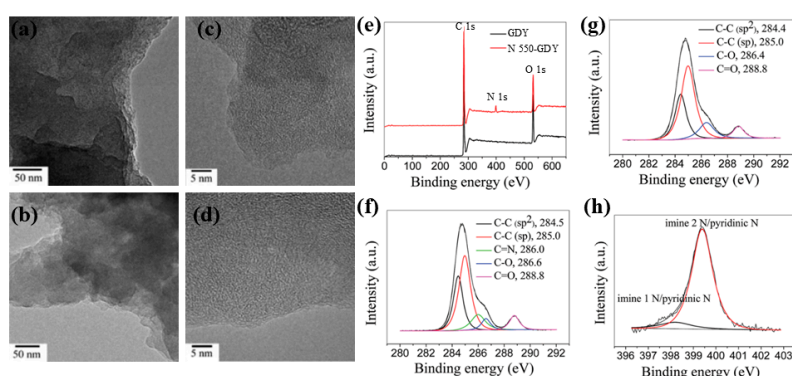


**Figure 6.** Structural characterizations of GDY and N-GDY. Transmission electron microscopy (TEM) images of (a) GDY and (b) N-GDY powder. HRTEM images of (c) GDY and (d) N-GDY powder; (e) X-ray photoelectron spectrometry (XPS) spectra (survey) of GDY and N-GDY. XPS C 1s spectra of (f) N-GDY and (g) GDY; (h) XPS N 1s spectrum of N-GDY. The C 1s peak of GDY can be split into four Lorentzian peaks at 284.4, 285.0, 286.4 and 288.8 eV [84–87]. The C 1s peak of N-GDY can be split into five Lorentzian peaks at 284.5, 285.0, 286, 286.6 and 288.8 eV [84,85]. The N 1s peak can be split into two Lorentzian peaks at 398.2 and 399.4 eV (reproduced with permission from [83]. Copyright The Royal Society of Chemistry, 2014).

### 3. Theoretical Predictions

2D full-carbon materials such as graphene [88–90] have been widely applied in electrochemical energy conversion devices such as fuel cells and metal–air batteries for their extraordinary catalytic properties towards the ORR, OER and HER processes and their low cost, easy synthesis and well-defined 2D planarity. In particular, the 2D electron-rich full-carbon framework material GDY with adjustable electronic structure and uniformly distributed porous structure has developed rapidly in the field of electrocatalysis in recent years. The functionalization methods of the GDY include metal-atom anchoring and nonmetallic-atom doping, which create ideal conditions for its better electrocatalysis performances. On one hand, single-atom (metal atom) catalysts have the greatest utilization efficiency of metal atoms and high-efficiency catalytic ability. Meanwhile, the variability of both the metal atoms and the supports provides a choice for its cost control. Therefore, this kind of catalyst with isolated metal atoms anchored on the support as the catalytic active centers [91] has attracted extensive attention and received in-depth research. The large triangular holes periodically arranged in the structure contribute to a relatively large specific surface area and the uneven charge distribution of the GDY are conducive to the anchoring of the single metal atom [33,92]. On the other hand, the introduction of nonmetallic-atom into the structure of GDY contributes to the modulation of the electronic structure and the control of performance, further providing the required properties for many

electrocatalytic processes with application significance. Below, the theoretical research progresses of metal-atom-anchored GDY catalysts and nonmetallic-atom-doped GDY catalysts for electrocatalytic applications will be discussed.

### 3.1. ORR

#### 3.1.1. Metal-Atom-Anchored GDY Electrocatalysts

GDY is a unique platform for synthesizing well-ordered and uniformly distributed metal-atom catalysts with high catalytic activity toward ORR electrocatalysis. With the theoretical studies based on the dispersion-corrected density functional calculation (DFT-D), Lu et al. [93] systematically studied the anchoring of noble-metal (NM) atom (Pd, Pt, Rh and Ir) on the surface of GDY, including the analysis of the geometric adsorption structure and embedded adsorption energy, electronic structure and frontier molecular orbitals. The NM atom is embedded in the 18C hexagon of GDY and has the largest adsorption energy at the large ring angle position of GDY. The adsorption energies of the four NM atoms of Pd, Pt, Rh and Ir are  $-3.12$  eV,  $-4.20$  eV,  $-4.41$  eV and  $-5.27$  eV, respectively and the mobility barrier energy increases with the embedded adsorption energy. The GDY anchored by Rh and Ir atoms, considered as the catalytic active centers, have potential catalytic application prospects. Moreover, the GDY anchored by the Rh atom has the strong electron-donating ability and the stable oxidation state of Rh, showing its great potential for ORR electrocatalysis [94].

In addition to the above-mentioned NM atoms, theoretical simulations have been also carried out on other transition metal atoms anchored on the surface of GDY for ORR catalytic activities. Feng et al. [95] used DFT as the theoretical guide to study the principle, process and activity of ORR catalysis of isolated transition metal (TM) atom supported by GDY (TM@GDY) in alkaline media. The ORR free energy diagrams (Figure 7a–c) of Ni atom anchored GDY (Ni@GDY), Pd atom anchored GDY (Pd@GDY) and Pt atom anchored GDY (Pt@GDY) show their four-electron ORR pathways. When the electrode potential reaches a certain value, the ORR process could occur spontaneously. The rate limiting step of the Ni@GDY is the last step ( $*\text{OH} \rightarrow \text{OH}^-$ ), while the rate limiting step of Pt@GDY is the first step ( $\text{O}_2 \rightarrow *\text{OOH}$ ). The ORR overpotential of Ni@GDY and Pt@GDY are equal to 0.44 V which is less than that of Pt (0.45 V) [96], demonstrating its remarkable ORR catalytic performance. Pd@GDY has a relatively high overpotential of 0.75 V, showing its relatively poor ORR catalytic performance. Meanwhile, the TM atoms are reactive sites because  $*\text{OOH}$ ,  $*\text{O}$  and  $*\text{OH}$  are adsorbed on Ni, Pd and Pt atoms (Figure 7d–f), and the adsorption free energy of  $*\text{O}$  species is generally larger than that of  $*\text{OOH}$  and  $*\text{OH}$  [96,97].

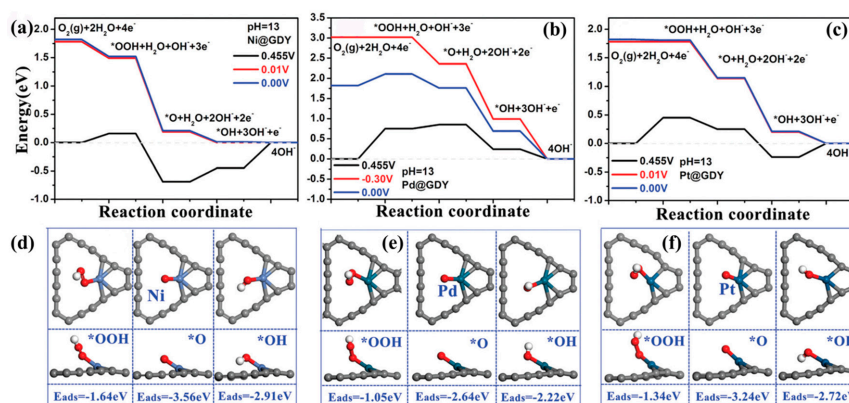


**Figure 7.** ORR free energy and intermediate adsorption diagrams of metal-atom-anchored GDY. The ORR free energy diagrams of (a) Ni@GDY, (b) Pd@GDY and (c) Pt@GDY. Optimized adsorption structures for  $*\text{OOH}$ ,  $*\text{O}$  and  $*\text{OH}$  on (d) Ni@GDY, (e) Pd@GDY and (f) Pt@GDY monolayers. The gray, red and white balls represent C, O and H atoms, respectively (reproduced with permission from [95]. Copyright The Royal Society of Chemistry, 2019).

### 3.1.2. Nonmetallic-Atom-Doped GDY Electrocatalysts

The ORR is the central reaction of the fuel cell [98] but its inherent slow response limits the overall performance [99,100]. To date, N-doped graphite carbon material including activated carbon, carbon nanotubes and graphene [72,101–103] have demonstrated to be the effective ORR catalysts. In this respect, the ORR process of N-atom-doped GDY on the cathode of a fuel cell was also discussed in many studies [104–111]. The ORR mechanism of N-doped GDY was investigated by using the first principles calculations. The kinetically most favorable and efficient four-electron reaction pathway ( $O_2 \rightarrow OOH \rightarrow O + H_2O \rightarrow OH \rightarrow H_2O$ ) was adopted [104]. The site-specific N doping of GDY including gap-N, sp-N (I) and sp-N (II)-doped GDY (Figure 8a) was systematically investigated as ORR electrocatalysts via DFT [108]. The adjacent sp-C atoms are activated as centers of ORR electrocatalytic process because the charge redistribution is caused by the doping of N atoms. Through the analysis of both dissociation (Figure 8b) and association mechanisms (Figure 8c) of  $O_2$  on pure GDY and three types of N-doped GDY catalysts, it is found that the doping of N atom has significant contributions to the amelioration of onset electrode potential of ORR electrocatalytic. For sp-N (I) GDY, the dissociation mechanism of  $O_2$  plays a leading role with its negligible dissociation barrier (0.04 eV) and relatively higher onset potential (0.51 V). Among the three types of N doping, in addition to sp-N (I) GDY, the onset potential of ORR in the association mechanism is higher than that in the dissociation mechanism. Of particular interest, the sp-N (II) doping provides the most significant ORR performance improvement by increasing the onset potential to 0.76 V, which is even comparable to that of noble metal Pt (1 1 1) catalyst (0.78 V) [96].

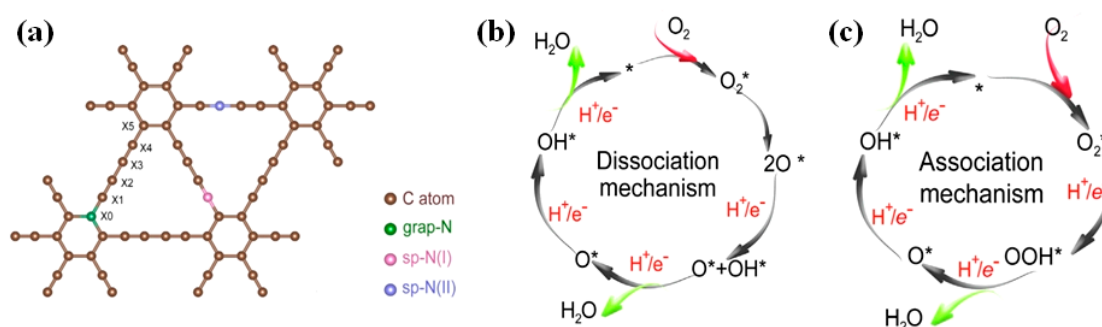


**Figure 8.** Geometric structure and oxygen reduction reaction (ORR) mechanisms of N-atom-doped GDY. (a) Three types of N-atom-doped GDY; (b) ORR-dissociation mechanism diagram; (c) ORR-association mechanism diagram (reproduced with permission from [108]. Copyright Science China Press, 2019).

In another study [105], special attention was paid to the ORR catalytic performances of three co-doped GDY, which were  $B_bN_{1(2)-}$ ,  $B_bN_{1(B)-}$  and  $B_bN_{2(1)-}$ -doped GDY, respectively (Figure 9a–c). All of the reaction steps are exothermic at the electrode potential of 0.00 V and when the electrode potential is higher than 0.66 V, some reaction steps become endothermic. The  $B_bN_{1(2)-}$ -doped GDY catalyst exhibits the best catalytic ability because its ORR overpotential (0.57 V) is lower than that of  $B_bN_{1(B)-}$ -doped GDY (0.61 V) and  $B_bN_{2(1)-}$ -doped GDY (0.64 V) (Figure 9d–f). Meanwhile, the GDY catalyst doped with  $B_bN_1$  has two active sites with almost the same catalytic activity, one of which is the B atom and the other is the  $C_2$  atom that has the closest positive charge to the N atom.  $*OOH$ ,  $*O$  and  $*OH$  are adsorbed on the B and  $C_2$  atoms and the adsorption energy values on the B and  $C_2$  atoms are approximately the same. While the  $C_1$  atoms act as active sites on  $B_bN_2$ -doped GDY because the  $*OOH$ ,  $*O$  and  $*OH$  occupy the top site of the  $C_1$  atoms that are directly bonded to the N and B atoms (Figure 9g–i). In general, the ORR performance of the ideal nonmetallic-atom-doped GDY catalyst is comparable to that of Pt-based materials. These results provide useful theoretical and research directions for the design of efficient and stable nonmetallic-atom-doped GDY catalysts for ORR electrocatalysis in the future.

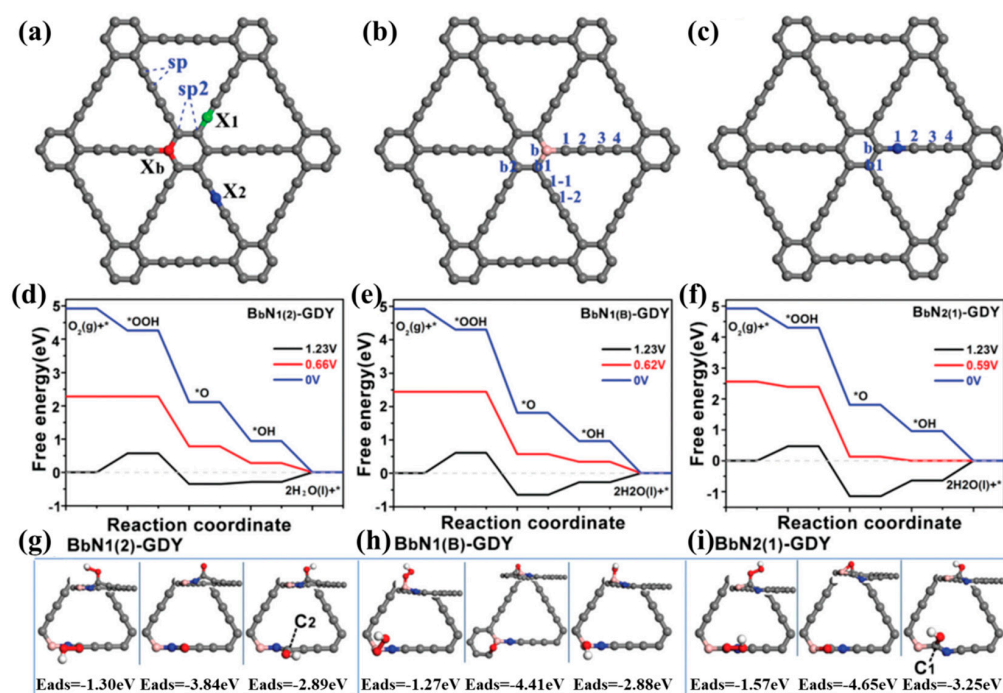


**Figure 9.** Geometric structures, free energy and intermediate adsorption diagrams of heteroatom-doped GDY. Geometric structures of (a) single-heteroatom-doped GDYs, (b)  $B_bN_y$ -doped GDY and (c)  $B_zN_1$ -doped GDY monolayers. Free energy diagrams for (d)  $B_bN_{1(2)}$ -, (e)  $B_bN_{1(B)}$ - and (f)  $B_bN_{2(1)}$ -doped GDY sheets. The optimized adsorption structures of  $^*OOH$ ,  $^*O$  and  $^*OH$  and the corresponding adsorption energy on (g)  $B_bN_{1(2)}$ -, (h)  $B_bN_{1(B)}$ - and (i)  $B_bN_{2(1)}$ -doped GDY monolayers. Gray, pink, blue, red and white balls represent C, B, N, O and H atoms, respectively (reproduced with permission from [105]. Copyright The Royal Society of Chemistry, 2019).

### 3.2. HER

#### Metal-Atom-Anchored GDY Electrocatalysts

The ORR is of pivotal significance for fuel cells and metal–air batteries. Similarly, the HER through electrocatalytic water splitting is considered as a promising approach to the production of clean hydrogen [112–114]. Recently, several research groups have studied the metal-atom-anchored GDY catalysts for HER electrocatalysis applications with the support of theoretical calculations. The bonding and anti-bonding orbitals near the Fermi level ( $E_F$ ) of zero-valence molybdenum-atom anchored GDY ( $Mo^0/GDY$ ) indicate that Mo is the active site and the Mo site as the electron-rich center can transfer charge and modifies the charge distribution from the C site to achieve effective electron transfer and stable adsorption of HER. In another study [62], the Pt atoms are anchored on GDY through the coordination interaction with the alkynyl C atoms in GDY, forming a five-coordinated  $C1-Pt-Cl_4$  species in Pt-GDY1 and a four-coordinated  $C_2-Pt-Cl_2$  species in Pt-GDY2. The interaction of Pt 5d orbital with the 1s orbital of H atom is favorable for transferring electrons to H atom, and the total unoccupied density of states of Pt 5d orbital is closely related to the formation of hydride [115]. Compared to Pt-GDY1, the relatively higher total unoccupied density of states of Pt 5d of Pt-GDY2 within the four-coordinated environment gives it a unique electronic structure that is conducive to its remarkable HER activity. As well-known, the Gibbs free energy ( $\Delta G_{H^*}$ ) is an important evaluation criterion for HER catalytic activity. When the Gibbs adsorption free energy of the reaction intermediate is closer to zero on the catalyst surface, the higher the HER electrocatalytic activity can be obtained [116,117]. Therefore, it is feasible to estimate the HER electrocatalytic activity of the catalyst by analyzing the  $\Delta G_{H^*}$  of the adsorption of H. For Pt-GDY1, a rather negative value of  $\Delta G_{H^*}$  ( $-0.653$  eV) indicates that the H atoms are too strongly adsorbed on the Pt active sites, which is also detrimental to the HER

process. However, the  $\Delta G_{H^*}$  of Pt-GDY2 is 0.092 eV, which is closest to the  $\Delta G_{H^*}$  of Pt metal surface ( $-0.09$  eV [118]), indicating its outstanding HER catalytic activity.

Not only DFT theory is used to study the HER electrocatalytic performance of the catalysts, the machine-learning (ML) [119] strategy is also used to provide the theoretical understanding and guidance for constructing metal-atom-anchored GDY catalysts for HER. Sun et al. comprehensively analyzed all TM and lanthanide (Ln) metals using DFT and ML strategies and found that C2 on the GDY chain is the most active electrically active site, showing both stable adsorption of H and desorption of  $H_2$  (Figure 10a,b). Simultaneously, the mapping of the chemisorption energy shows limited regulation with the number of d electrons, while the increase of chemisorption from 3d to 5d indicates that H coverage preference is decreasing (Figure 10c). Pt shows the greatest potential for electrocatalytic application to HER owing to its nearly zero-energy variation. Sm and Eu can adsorb the second H atom because they only require a small energy cost of less than 0.2 eV, and Eu-4f and Sm-4f orbitals have high electrical active for reduction based on electron depletion, making them effective electrocatalyst with excellent HER catalytic performance. For 3d metals, the continuous H adsorption and final desorption of  $H_2$  are both thermodynamically spontaneous. The formation cost of  $H_2$  follows the order of  $Fe > Co > Ni$ . It is worth noting that the very subtle energy changes displayed by Ni-atom anchored GDY catalyst during the HER process is evidence of its highly efficient HER activity (Figure 10d). Meanwhile, according to the energy cost of ( $2H^* \rightarrow *H_2$ ) is the main potential determination criterion for the 4d element, it can be concluded that Pd, Ag and Cd are energetically favorable candidates (Figure 10e). Only Pt and Hg show the spontaneous reaction trend of ( $2H^* \rightarrow *H_2$ ) and the higher energy cost of the remaining 5d is needed to form  $H_2$ , which represents poor HER performance (Figure 10f). In addition, compared to 3d metals, the energy variation of most 4d and 5d metals is larger than 0.4 eV, indicating the slightly lower HER efficiency, and its electroactivity follows the order of  $3d > 4d > 5d$ . The electrical activity demonstrated by DFT and ML have similarly trend, proving the capability of ML in predicting of electroactivity of novel catalysts (Figure 11). The application of new technology helps to discover more potential HER electrocatalysts with ideal performance and opens new opportunities for future design and synthesis of efficient metal-atom-anchored catalyst as well.

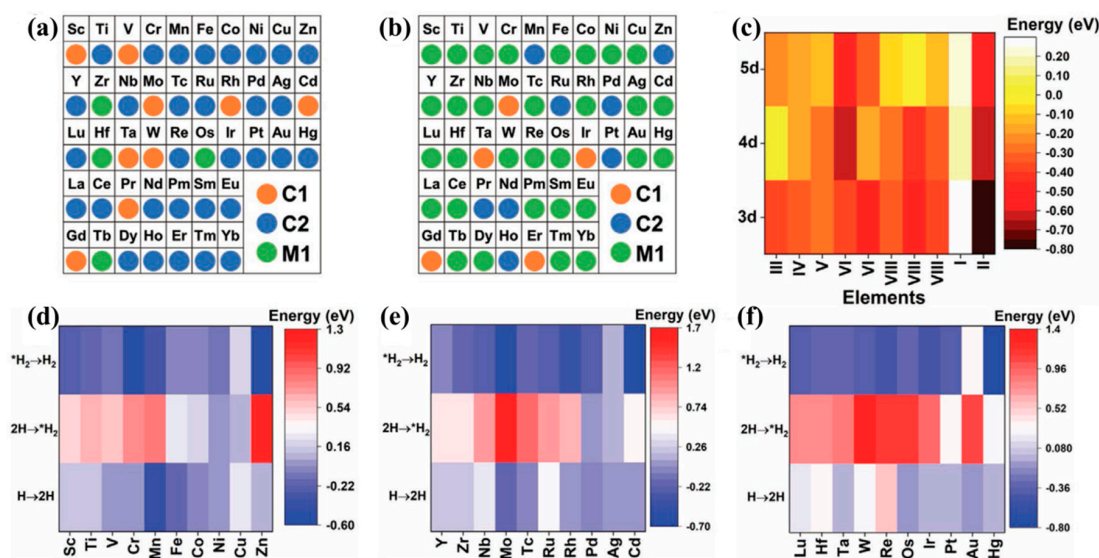


**Figure 10.** Density functional calculation (DFT-D) mapping of active site and reaction energy for metal-atom-anchored GDY catalysts. (a) Mapping of the preferable initial adsorption site for  $H^*$  in hydrogen evolution reaction (HER); (b) mapping of the final desorption site for  $H_2$  in HER; (c) mapping of the chemisorption energy for TM atom anchored GDY catalysts. Mapping of the reaction energy of HER for (d) 3d, (e) 4d and (f) 5d TM atom anchored GDY catalysts (reproduced with permission from [119]. Copyright Wiley-VCH, 2020).

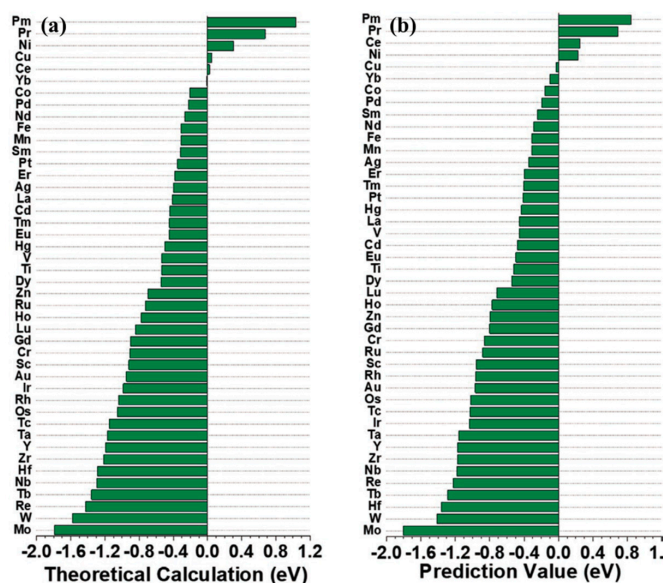


**Figure 11.** Prediction values of 2H adsorption energy calculated by (a) theoretical calculation and (b) machine learning (reproduced with permission from [119]. Copyright Wiley-VCH, 2020).

### 3.3. OER

#### Metal-Atom-Anchored GDY Electrocatalysts

As a semiconductor material [120,121], GDY has a natural and direct band gap of 0.52 eV (Figure 12a) [28,122]. This band gap can be reduced to 0.26 eV (Figure 12b) by the anchoring of Ni atoms on the surface of GDY [123], which effectively improves the conductivity and further accelerates the electrocatalytic reaction. The three possible adsorption sites of TM atoms (Sc to Zn and Pt) anchored on the surface of GDY were simulated [123], namely S1, S2 and S3 (Figure 12c). It is found that the TM atoms located at S1 automatically move to S2 after optimization, which indicates that the most stable and energetic adsorption site is S2. The high migration energy barrier (3.35 eV) of the NM atoms on the surface of GDY makes it extremely difficult for the anchored TM atoms to diffuse from its stable site to another site. As can be seen from Figure 13, the calculated overpotentials ( $\eta$ ) of Mn@GDY, Fe@GDY, Sc@GDY, Co@GDY, Cr@GDY, Ti@GDY and Cu@GDY are 1.81, 1.66, 1.68, 0.84, 1.80, 1.92 and 0.92 V, all of them need too much energy input to catalyze the OER processes. Meanwhile, the strong binding character will also poison the catalysts. Thus, these catalysts are not the ideal candidates for OER. Interestingly, only Ni@GDY and Pt@GDY that have more positive values of  $\Delta G_{\text{OH}^*}$  possess favorable values of 0.29 and 0.46 V for OER. This shows that Ni@GDY and Pt@GDY have promising potential in OER electrocatalysis.

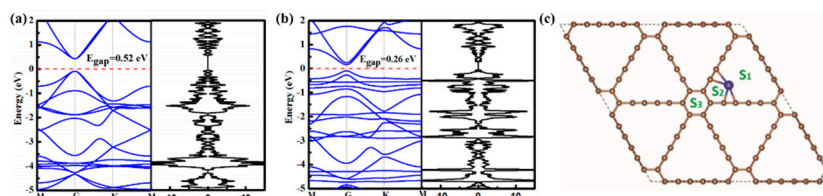


**Figure 12.** Band structures of the pristine and the TM-atom anchored GDY and different possible adsorption sites for the single TM-atoms supported on GDY. Electronic properties of band structures and density of states of (a) GDY monolayer and (b) Ni@GDY composite. The Fermi level is set to zero; (c) different possible adsorption sites for the single TM atoms supported on GDY: at the center of the holes (S1), at the corner of the holes (S2) and at the center of hexatomic ring (S3). (reproduced with permission from [123]. Copyright Wiley-VCH, 2019).

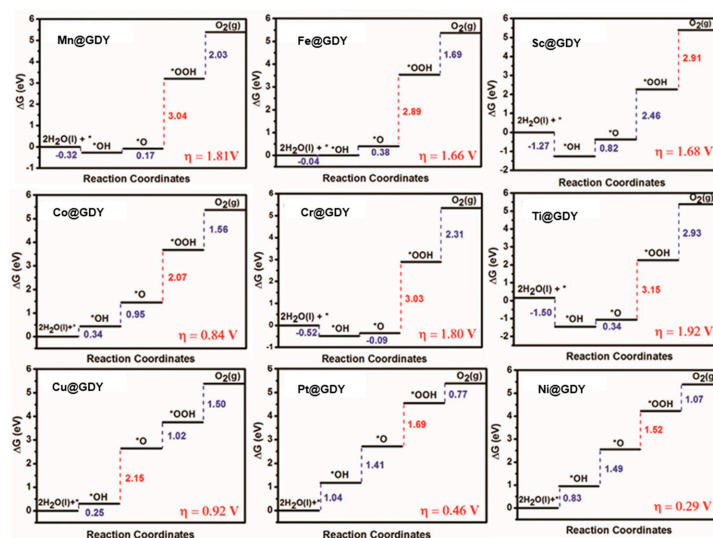


**Figure 13.** Calculated free energy diagrams of TM@GDY complex for OER under  $E = 0$  V, where the potential-determining step of the elementary reaction is marked in red (reproduced with permission from [123]. Copyright Wiley-VCH, 2019).

#### 4. Experimental Investigations

In fuel cells and metal–air batteries, the ORR, OER and HER processes require high-quality catalysts to obtain rapid reaction kinetics in order to play a role in practical electrocatalytic applications. Pt and Pt-supported alloy materials have long been regarded as the most effective electrocatalysts for their remarkable catalytic performance [124–126], but their high cost and poor durability have become the main development bottlenecks for their commercialization [127,128]. Under this circumstance, single-atom (metal atom) catalysts stand out and are regarded as highly effective catalysts that are expected to replace Pt-based catalysts. Among them, to increase the exposed active sites of the catalyst and obtain the maximum utilization efficiency of metal atoms and at the same time find an appropriate catalyst support to stably disperse and effectively anchor the metal atoms, are the strategy to obtain the metal-atom catalysts with stable and efficient catalytic capabilities [129–132]. Under the guidance of this strategy, GDY has been proposed as a suitable support for metal-atom catalysts for its rich  $C\equiv C$  bonds in the structure with higher degree of conjugation and chemical stability [28].

Moreover, low-cost nonmetallic electrocatalysts have been devoted to the development of various catalytic processes involving either oxidation or reduction reactions [133]. In particular, the carbon-based materials GDY, are ideal candidates for being the support for catalysts owing to their wide availability, corrosion resistance and unique surface and bulk properties. Simultaneously, the adjustability of the structure of GDY is a guarantee for the doping of nonmetallic-atom and the introduction of heteroatoms can enable the modulation of the electronic structure of GDY, and thus the electrocatalytic activity can be further improved [83]. The functionalization of GDY by nonmetallic-atom doping is expected to further promote the application of this multifunctional GDY material in the field of electrocatalysis. At the same time, these excellent catalysts contribute to the richness of electrocatalyst materials and further promote the development of the field of electrocatalysis. In the following, the experimental research progresses of metal atom anchored GDY catalyst and nonmetal atom-doped GDY catalyst for electrocatalytic applications will be discussed.

##### 4.1. ORR

###### 4.1.1. Metal-Atom-Anchored GDY Electrocatalysts

In view of the brilliant electrocatalytic properties of metal-atom-anchored GDY catalysts supported by theoretical calculations; several experimental studies have been carried out to explore its value in

the field of electrocatalysis. Iron (Fe) atoms are anchored on the surface of GDY by forming a covalent bond with the C atoms in the GDY framework, and the formed catalyst has high catalytic activity for ORR process comparable to the precious metal benchmark (commercial 20 wt% Pt/C catalyst [134]) in alkaline electrolytes [135]. The cyclic voltammetry (CV) results indicate that both the cathodic peak for O<sub>2</sub> reduction and peak current of Fe/GDY are close to that of 20 wt% Pt/C catalyst (Figure 14a), which shows that Fe/GDY catalyst has high ORR activity in alkaline solution. The value of onset potential ( $E_{\text{onset}}$ ) of Fe/GDY catalyst is approximately 0.21 eV (vs. RHE), which is close to that of Pt/C catalyst (0.20 eV (vs. RHE)) (Figure 14b). Moreover, the Fe/GDY catalyst has a Tafel slope (Figure 14c) value of about 63 mV dec<sup>-1</sup> in the high potential region, which is almost identical to that of commercial Pt/C catalysts (62 mV dec<sup>-1</sup> [136]). The stability test results show that the  $E_{\text{onset}}$  of the Fe/GDY catalyst has almost no change, the half-wave potential ( $E_{1/2}$ ) has only a slight negative shift while the  $E_{\text{onset}}$  and the  $E_{1/2}$  of Pt/C catalyst have undergone relatively large changes, indicating the superior stability of the Fe/GDY catalysts (Figure 14d) (Table 1). The better and beneficial stability of Fe/GDY catalyst may be also derived from the fact that the active sites in the catalyst are not easy to be oxidized or reduced, and the Fe atoms form coordination bonds with C atoms. It is worth knowing that the Fe/GDY catalyst with the high catalytic activity and stability facilitates 4e<sup>-</sup> ORR process while limiting the 2e<sup>-</sup> transfer reaction, and the high 4e<sup>-</sup> selectivity to ORR process is more conducive to the improvement of its electrocatalytic activity.

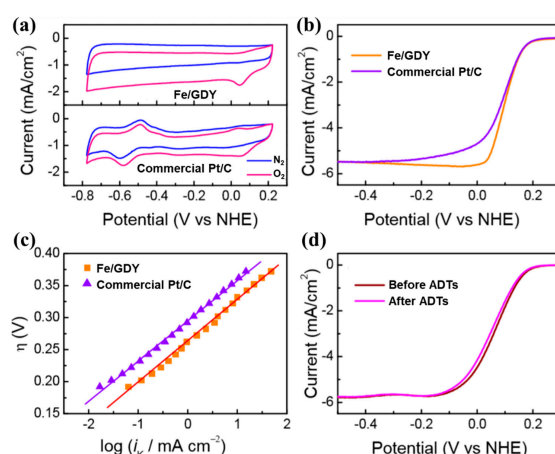


**Figure 14.** Electrochemical characterizations of Fe/GDY. (a) CV responses of the Fe/GDY catalyst and the commercial Pt/C catalyst in N<sub>2</sub>- and O<sub>2</sub>-saturated 0.1-M KOH solution at ambient temperature. The scanning rate was 50 mV/s. The loading of the Fe/GDY catalyst was 0.49 mg/cm<sup>2</sup>, and the loading of the Pt/C catalyst was 20 μg<sub>Pt</sub>/cm<sup>2</sup>; (b) RDE measurements in O<sub>2</sub>-saturated 0.1-M KOH solution for the Fe/GDY catalyst and the commercial 20 wt% Pt/C catalyst. The measurements were performed at a rotating speed of 1600 rpm and a scanning rate of 5 mV/s; (c) Tafel ORR plots obtained at the Fe/GDY and commercial 20-wt% Pt/C catalyst; (d) stability of the Fe/GDY catalyst to the ORR. The RDE responses were recorded in O<sub>2</sub>-saturated 0.1-M KOH solution at a rotating speed of 1600 rpm and a scanning rate of 5 mV/s before and after ADTs (reproduced with permission from [135]. Copyright American Chemical Society, 2018).

**Table 1.** Oxygen reduction reaction (ORR) performance of metal-atom-anchored GDY and nonmetallic-atom-doped GDY.

| Catalysts <sup>1</sup> | Synthesis Method           | $E_{\text{onset}}$<br>(V vs. RHE) | $E_{1/2}$<br>(V vs. RHE) | $I_d$<br>(mA cm <sup>-2</sup> ) | Tafel Slope<br>(mV dec <sup>-1</sup> ) | Ref.  |
|------------------------|----------------------------|-----------------------------------|--------------------------|---------------------------------|--|-------|
| Fe/GDY                 | chemical reduction         | 0.21                              | 0.1                      | 6.7 (0.1 V)                     | 63                                     | [135] |
| NGDY                   | high-temperature annealing | N/A                               | 0.87                     | 38.0 (0.75 V)                   | 60                                     | [82]  |
| NFGDY                  | high-temperature annealing | 1.0                               | 0.74                     | 4.5 (0 V)                       | N/A                                    | [79]  |

<sup>1</sup> electrolyte: 0.1-M KOH.

#### 4.1.2. Nonmetallic-Atom-Doped GDY Electrocatalysts

The excellent ORR catalytic activity, high stability and high methanol tolerance of nonmetallic-atom-doped GDY catalysts were also experimentally confirmed. For example, sp-N atom-doped few-layer GDY (NGDY) catalysts with outstanding ORR performance were successfully prepared [82]. The cathode current density provided by NGDY is most consistent with Pt/C and the optimal sp-N-doped GDY exhibits comparable catalytic activity to Pt/C, with  $E_{1/2}$  of 0.87 V and  $J_k$  of  $38.0 \text{ mA cm}^{-2}$  at 0.75 V in the alkaline solution. The site-specific sp-N atom doping is most favorable for  $\text{O}_2$  adsorption and electron transfer on the catalyst surface compared to other N-doped forms. With the increase of the concentration of sp-N atom in alkaline and acidic solutions, the current density increases monotonically, confirming that the sp-N atom is the most important active N-doping form for the ORR electrocatalysis.

In addition to the single N-atom doping form, the N atom and fluorine (F) atom co-doped GDY catalyst also exhibits enhanced ORR catalytic activity, and it shows a much better stability with a higher tolerance to methanol crossover and CO poisoning effects than the commercial Pt/C [79]. The NFGDY exhibited an  $E_{\text{onset}}$  of 1.0 V vs. RHE and a disk current ( $I_d$ ) of  $4.5 \text{ mA cm}^{-2}$  at 0 V vs. RHE (Figure 15a), which are comparable to those of Pt/C ( $E_{\text{onset}} = 1.0 \text{ V}$ ,  $I_d = 4.3 \text{ mA cm}^{-2}$  at 0 V vs. RHE). The average electron transfer number of NFGDY during the reaction is 4.2 for a wide potential range from 0 V to 0.8 V (vs. RHE), suggesting complete selectivity toward total oxygen reduction (Figure 15b). The NFGDY modified electrode shows a 20 mV negative shift in  $E_{1/2}$ , but no negative shift in  $E_{\text{onset}}$  and decline in the limiting current density are observed (Figure 15c). The NFGDY has no response specific to methanol, but the catalytic activity of Pt/C drops severely (Figure 15d). These data indicated that NFGDY has a promising long-term operational stability. Notably, in terms of its onset potential and limiting current density, the as-prepared NFGDY exhibits comparable performance to commercial Pt/C both in half-cell Zn–air battery. The remarkable synergistic effect produced by the co-doping of N and F atoms endows this new type of nonmetallic-atom-doped GDY electrocatalyst an efficient and stable ORR catalytic performance.

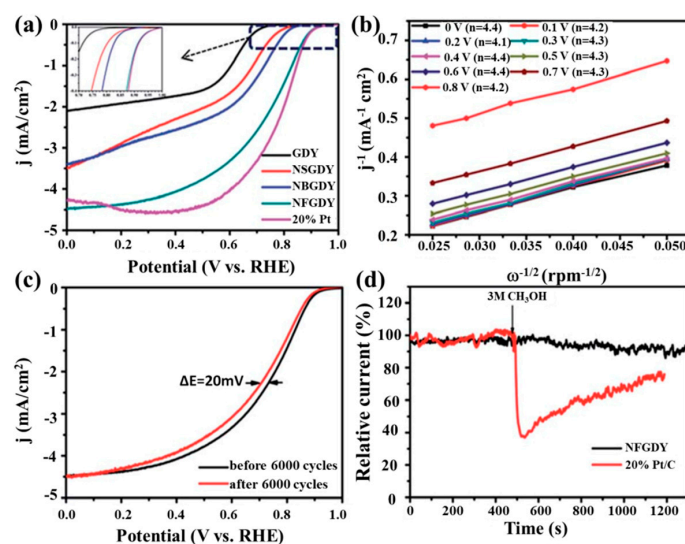


**Figure 15.** ORR electrochemical characterizations of polyatomic co-doped GDY. (a) LSV curves of GDY, NSGDY, NBGDY and NFGDY obtained from RDE measurements at 1600 rpm at a scan rate of  $10 \text{ mV s}^{-1}$  in  $\text{O}_2$ -saturated 0.1-M KOH; (b) Koutecky–Levich (K–L) plots of NFGDY calculated at different potentials; (c) stability tests of NFGDY at 1600 rpm before and after 6000 continuous CV cycles from  $-0.05$  to  $1.15 \text{ V}$  (vs. RHE) at a scan rate of  $200 \text{ mV s}^{-1}$ ; (d) methanol-tolerance evaluation of NFGDY tested by the current–time chronoamperometric responses (20% Pt/C is used for comparison) (reproduced with permission from [79]. Copyright The Royal Society of Chemistry, 2016).

## 4.2. HER

## Metal-Atom-Anchored GDY Electrocatalysts

The unique and precise chemical and electronic structure of the GDY support allows for the anchoring of dispersed metal atoms and can maximize the use of metal atoms while increasing as many active sites as possible. The strong p-d coupling between the metal atoms and the C atoms in GDY activates the effective proton electronic exchange between the active site and the support, suppressing the free energy of HER close to zero. Taking advantage of this, the isolated and dispersed Ni and Fe atoms anchored GDY catalysts were developed [67] and these catalysts exhibited excellent HER performance (Table 2) among all reported nonprecious HER single-atom catalysts and most of the state-of-the-art bulk catalysts. Clearly, the Fe atom anchored GDY (Fe/GDY) catalyst exhibits the best HER activity with the smallest onset overpotential of 9 mV and an overpotential of 66 mV at 10 mA cm<sup>-2</sup>, which is smaller than that of Ni atom anchored GDY (Ni/GDY) (88 mV), GD foam (GDF) (578 mV) and carbon cloth (CC) (642 mV) (Figure 16a). The Fe/GDY and Ni/GDY catalysts show very small Tafel slopes of 37.8 and 45.8 mV dec<sup>-1</sup> (Figure 16b), respectively, which are comparable to that of Pt/C (33.9 mV dec<sup>-1</sup>). According to the values of the Tafel slope, the Volmer-Heyrovsky mechanism is operative during the HER process. (If the value of Tafel slope is 120 mV dec<sup>-1</sup>, the Volmer reaction is the rate-determining step. If the Tafel slope is 40 mV dec<sup>-1</sup> or 30 mV dec<sup>-1</sup>, the speed-determining steps are Heyrovsky and Tafel reactions, respectively). TOF is the best parameter to compare the intrinsic activity of different catalysts [137]. The TOF of Ni/GDY and Fe/GDY are 1.59 and 4.15 s<sup>-1</sup> (Figure 16c) at 100 mV, which are much higher than those of the other recently reported electrocatalysts such as CoP (0.046 s<sup>-1</sup>) [115] and Ni<sub>2</sub>P (0.015 s<sup>-1</sup>) [138]. In addition, the mass activity is an important evaluation standard for characterizing catalytic performance in practical applications [115]. The mass activity of Fe/GDY and Ni/GDY on HER are significantly better than that of commercial Pt when normalized with respect to their respective loads (Figure 16d). Remarkably, after 5000 potential cycling tests, the polarization curves of Ni/GDY (Figure 16e), Fe/GDY (Figure 16f) remain unchanged in current density, which are superior to commercial Pt/C in terms of stability. The loss of geometric exchange current density of Ni/GDY and Fe/GDY are negligible even at 116 h and 60 h of constant electrolysis. Using the unique chemical structure and strong p-d coupling of the GDY, the uniform porosity of GDY also contributes to the excellent HER performance of the metal-atom anchor catalyst. The novel zero valence palladium atom anchored GDY (Pd<sup>0</sup>/GDY) ultrathin nanosheet prepared by electrochemical-deposition method results in a highly active and stable HER catalytic process when used as a three-dimensional flexible hydrogen-evolving cathode [68]. The porosity of Pd<sup>0</sup>/GDY catalyst facilitates rapid mass transfer and gas escape, ensuring sufficient contact between the electrolyte, which is the guarantee of its outstanding performance as HER catalysts.

Table 2. HER performance of metal-atom-anchored GDY.

| Catalysts                         | Synthesis Method           | $\eta$<br>At 10 mA<br>cm <sup>-2</sup> (mV) | $E_{\text{onset}}$<br>(V vs. RHE) | $j_0$<br>(mA cm <sup>-2</sup> ) | Tafel Slope<br>(mV dec <sup>-1</sup> ) | TOF (s <sup>-1</sup> ) | Mass<br>(A mg <sub>metal</sub> <sup>-1</sup> ) | Ref.  |
|-----------------------------------|----------------------------|---|-----------------------------------|---------------------------------|--|------------------------|--|-------|
| Ni/GDY <sup>1</sup>               | electrochemical-deposition | 86  | 23                                | 0.25 (0 V)                      | 45.8                                   | 1.59 (0.1 V)           | 16.6 (0.2 V)                                   | [67]  |
| Fe/GDY <sup>1</sup>               | electrochemical-deposition | 66  | 9                                 | 0.29 (0 V)                      | 37.8                                   | 4.15 (0.1 V)           | 80.0 (0.2 V)                                   | [67]  |
| Pd <sup>0</sup> /GDY <sup>1</sup> | electrochemical-deposition | 55  | 11                                | 0.28 (0 V)                      | 47                                     | 16.7 (0.1 V)           | 61.5 (0.2 V)                                   | [68]  |
| Ru/GDY <sup>1</sup>               | in situ reduction          | 44  | N/A                               | 0.70 (0 V)                      | 30                                     | 8.45 (-0.1 V)          | 15.88 (0.15 V)                                 | [64]  |
| Cu@GDY-Co <sup>2</sup>            | absorption-reduction       | 63  | N/A                               | N/A                             | 41.7                                   | N/A                    | N/A  | [139] |

<sup>1</sup> electrolyte: 0.5-M H<sub>2</sub>SO<sub>4</sub>. <sup>2</sup> electrolyte: 1.0-M KOH.

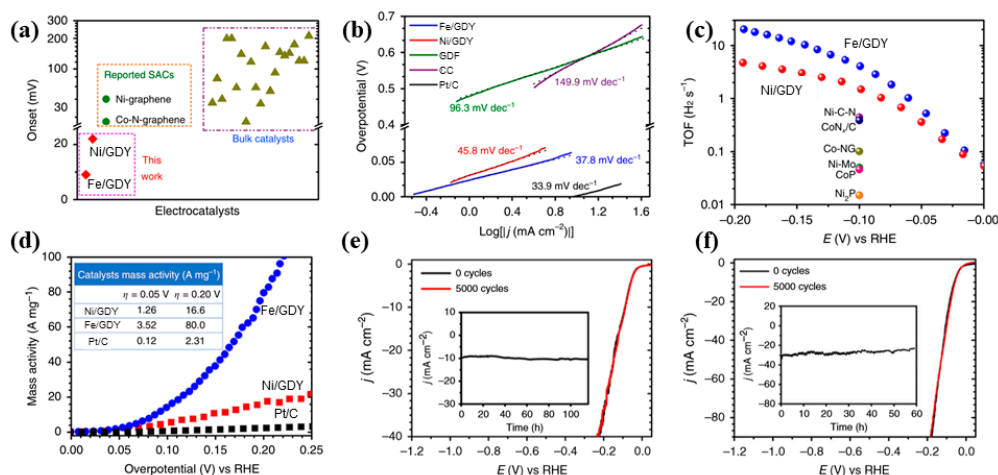


**Figure 16.** Electrochemical characterizations of Ni/GDY and Fe/GDY. (a) Onset values at  $10 \text{ mA cm}^{-2}$  of Ni/GDY and Fe/GDY (red square) along with other nonprecious single-atom HER catalysts (green circle) and several bulk catalysts (olive triangle); (b) Tafel plots of the presented data in (a); (c) TOF values of Fe/GDY (blue dot) and Ni/GDY (red dot) together with several state-of-the-art HER electrocatalysts; (d) mass activities of Ni/GDY, Fe/GDY and Pt/C (inset: mass activities obtained at overpotentials of 0.05 V and 0.20 V). Stability tests of (e) Ni/GDY and (f) Fe/GDY (insets: respective time-dependent current density curves) (reproduced with permission from [67]. Copyright Springer Nature, 2018).

### 4.3. OER

#### 4.3.1. Metal-Atom-Anchored GDY Electrocatalysts

To date, the development of dual-function electrocatalysts capable of driving both HER and OER processes with a small applied voltage can better meet the requirements in practical applications but remains challenges. Inspired by the fact that ruthenium (Ru) supported oxides are generally considered to be effective electrocatalysts for acidic OER and the fact that GDY can be applied as an efficient and stable catalyst support for anchoring metal atoms, Ru atom anchored GDY (Ru/GDY) catalyst has been prepared by the in-situ reduction method and shows outstanding catalytic activity and stability in both OER and HER processes in acid solution [64]. The Ru/GDY shows the excellent OER activity with the low overpotential of 531 mV to reach  $10 \text{ mA cm}^{-2}$  and the small Tafel slope of  $100 \text{ mV dec}^{-1}$  and the big  $j_{\text{mass}}$  of  $9.03 \text{ A mg}_{\text{metal}}^{-1}$  (at the 2.0 V), which is 451 times larger than RuO<sub>2</sub> ( $0.02 \text{ A mg}_{\text{metal}}^{-1}$ ). The Ru/GDY shows the excellent HER activity with the overpotential of 44 mV at  $10 \text{ mA cm}^{-2}$  and the fastest reaction rate with the smallest Tafel slope of  $30 \text{ mV dec}^{-1}$ . The mass activity polarization curves further confirmed the superior catalytic activity of Ru/GDY, for example, At the overpotential of 150 mV, Ru/GDY shows the mass activity of  $15.88 \text{ A mg}_{\text{metal}}^{-1}$ , which is 15.88-times larger than 20 wt% Pt/C ( $1.00 \text{ A mg}_{\text{metal}}^{-1}$ ) (Table 3). Remarkably, the strong p-d coupling between Ru atoms and neighboring C atoms produces an intrinsic electron compensation reservoir that generates an abnormally high oxidation of anchored Ru atoms, making Ru atom to be a unique electron-mediating-vehicle (EMV) with a dynamic self-modification for fast reversible redox-switching. Despite of the excellent performance of Ru/GDY catalyst for OER and HER, the Ru/GDY is also used as both anode and cathode for overall water decomposition in acidic media. The electrode only needs 1.81 V of the cell voltage to deliver  $10 \text{ mA cm}^{-2}$ , which confirms its excellent electrocatalytic activity. In another recent study, Shi et al. described a new strategy that utilizes strong electronic perturbation effect to stabilize ultrasmall Co clusters, which adopt GDY nanoarray as support material (Cu@GDY-Co) [139]. As a self-standing bifunctional electrocatalysts for overall water splitting, the Cu@GDY-Co electrocatalyst displays superior activities for both OER (with the overpotential of 234 mV at  $10 \text{ mA cm}^{-2}$  and the Tafel slope value of  $51.7 \text{ mV dec}^{-1}$ ) and HER (with the overpotential of 63 mV at  $10 \text{ mA cm}^{-2}$  and the Tafel slope value of  $41.7 \text{ mV dec}^{-1}$ ). Given the high HER and OER performances, the Cu@GDY-Co catalyst was

directly used as both the cathode and anode to assemble a two-electrode alkaline electrolyzer for overall water splitting (Figure 17a). As shown in Figure 17b,c, this device delivers current densities of  $10 \text{ mA cm}^{-2}$  and  $100 \text{ mA cm}^{-2}$  with a cell voltage of 1.53 V and 1.70 V, respectively, which are even higher than that of  $\text{IrO}_2(+)//\text{Pt}(-)$  electrode. Meanwhile, the electrolyzer maintains a stable cell voltage at different current densities ranging from 10 to  $100 \text{ mA cm}^{-2}$ , indicating the good stability of Cu@GDY-Co electrode. Benefiting from the unique electronic property and acetylenic bond structure in GDY, ultrasmall Co clusters can be effectively stabilized on the surface of GDY, ensuring the efficient expose of catalytic activity sites. At the same time, the intimate electronic interaction between GDY and ultrasmall Co clusters significantly reduces the free energy of intermediates in the electrolysis of water, resulting in the improvement of intrinsic catalytic activity. This dual-function catalyst with extraordinary OER and HER catalytic activity guarantees the potential for commercial application and is conducive to the further development of metal-atom-anchored GDY catalysts in the field of dual-function electrocatalysis.

**Table 3.** OER performance of metal-atom-anchored GDY and nonmetallic-atom-doped GDY.

| Catalysts <sup>1</sup>    | Synthesis Method              | $\eta$<br>At 10 mA<br>$\text{cm}^{-2}$ (mV) | $j_0$<br>( $\text{mA cm}^{-2}$ ) | Tafel Slope<br>( $\text{mV dec}^{-1}$ ) | TOF<br>( $\text{s}^{-1}$ ) | Mass<br>( $\text{A mg}_{\text{metal}}^{-1}$ ) | Ref.  |
|---------------------------|-------------------------------|---|----------------------------------|---|----------------------------|---|-------|
| Ru/GDY <sup>1</sup>       | in situ reduction             | 531   | 0.084 (0 V)                      | 100                                     | 7.09 (2.0 V)               | 9.03 (2.0 V)                                  | [64]  |
| Cu@GDY-Co <sup>2</sup>    | absorption–reduction          | 234   | N/A                              | 51.7                                    | N/A                        | N/A   | [139] |
| NSFLGDY-900 <sup>2</sup>  | high-temperature<br>annealing | 299   | 47.2 (1.6 V)                     | 62                                      | N/A                        | N/A   | [78]  |
| NSFLGDY-900a <sup>2</sup> | high-temperature<br>annealing | 308   | 35.7 (1.6 V)                     | 66                                      | N/A                        | N/A   | [78]  |
| NSFLGDY-900b <sup>2</sup> | high-temperature<br>annealing | N/A   | 4.6 (1.6 V)                      | 79                                      | N/A                        | N/A   | [78]  |

<sup>1</sup> electrolyte: 0.5-M  $\text{H}_2\text{SO}_4$ . <sup>2</sup> electrolyte: 1.0-M KOH.

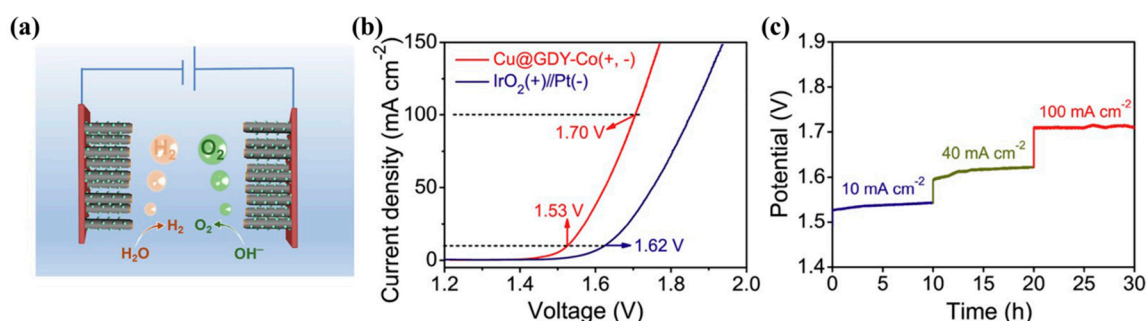


**Figure 17.** Overall water splitting schematic illustration and electrochemical characterizations of Cu@GDY-Co. (a) Schematic illustration of the electrolyzer using Cu@GDY-Co as both cathode and anode; (b) polarization curves for overall water splitting; (c) chronopotentiometric curve of water electrolysis recorded at the current density of 10, 40 and  $100 \text{ mA cm}^{-2}$  (reproduced with permission from [139]. Copyright Elsevier, 2020).

#### 4.3.2. Nonmetallic-Atom-Doped GDY Electrocatalysts

Carbon-rich nanomaterials [140] can be used as high-quality OER electrocatalyst for their definable active centers, controllable nanostructures and excellent chemical stability. The application of nonmetallic-atom-doped GDY catalysts in the OER electrocatalytic process has been also explored. For instance, the high spin of the active site of the sp-N-doped GDY catalyst contributes to its high OER catalytic activity, making its catalytic activity comparable to that of  $\text{RuO}_2$  [107]. With respect to the individual atom doping, polyatomic co-doped carbon materials have more advantages for enhancing the OER performance. Zhao et al. [78] used melamine and dibenzyl sulfide as doping sources to prepare few-layer GDY catalyst with single nonmetallic-atom doping and co-doping of N atom and S atoms at a high temperature of  $900 \text{ }^\circ\text{C}$  (NSFLGDY-900 (1.0 g of melamine and 2.0 g of

dibenzyl sulfide)) through several simple experimental steps. Meanwhile, the NSFLGDY-900a (1.0 g of melamine and 1.0 g of dibenzyl sulfide) and the NSFLGDY-900b (0.5 g of melamine and 2.0 g of dibenzyl sulfide) catalyst had been also prepared for cross-referenced catalysts. In this way, the OER performances of the N and S atom co-doped GDY catalysts and the respective contributions of the N atom and S atom in synergistically and positively affecting the OER catalytic performance had been investigated. The co-doped NSFLGDY-900 catalyst exhibits outstanding OER performance with the overpotential of 299 mV at 10 mA cm<sup>-2</sup>, which is smaller than that of RuO<sub>2</sub> (305 mV) catalyst and the highest current density of 47.2 mA cm<sup>-2</sup> at a potential of 1.6 V (vs RHE), which surpasses that of RuO<sub>2</sub> (33.9 mA cm<sup>-2</sup>) catalyst (Figure 18a,b). Meanwhile, the NSFLGDY-900 has a lower Tafel slope than RuO<sub>2</sub> catalyst, further indicating its faster OER kinetic process (Figure 18c). Figure 18d–f demonstrates that the introduction of sp-N atom significantly reduces the overpotential of the catalyst and the subsequent introduction of S atom contributes to the improvement of the OER current density. This multi-atom synergistic effect has a significant contribution in regulating the activity of the catalyst, opening a new way for the further design and guidance of new carbon-based catalysts for efficient electrocatalytic process.

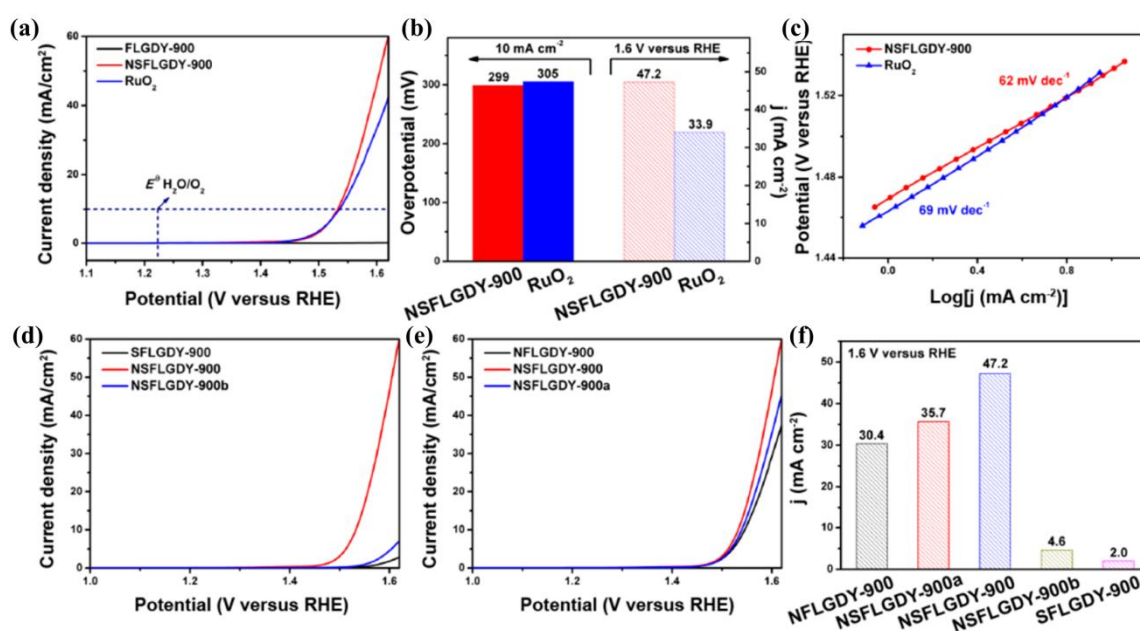


**Figure 18.** OER electrochemical characterizations of polyatomic co-doped GDY. (a) Polarization curves of FLGDY-900, NSFLGDY-900 and RuO<sub>2</sub> catalysts; (b) corresponding overpotential and current density of NSFLGDY-900 and RuO<sub>2</sub> catalysts; (c) Tafel plots of NSFLGDY-900 and RuO<sub>2</sub> catalysts; (d) polarization curves of SFLGDY-900, NSFLGDY-900 and NSFLGDY-900b catalysts; (e) polarization curves of NFLGDY-900, NSFLGDY-900 and NSFLGDY-900a catalysts; (f) current density of catalysts at 1.6 V (vs. RHE) (reproduced with permission from [78]. Copyright American Chemical Society, 2019).

## 5. Conclusions and Perspectives

In conclusion, with the continuous expansion of the demand of sustainable clean energy, electrocatalysis has increasingly become a research focus in the field of catalysis and the desire for electrocatalysts that can be easily prepared with long-term stability and excellent catalytic activity is also increasing gradually. Under such circumstances, the highly conjugated, uniformly porous, electron-rich 2D full-carbon material GDY, with high structural adjustability [141] and high modifiability, becomes one of the best choices for constructing efficient and stable electrocatalyst with commercial application prospects.

In brief, this review presents an overview of the recent achievements in the synthesis methods and applications of GDY as the core material to construct catalysts anchored by metal atoms and doped

with nonmetallic atoms in the field of electrocatalysis. For the preparation of metal-atom-anchored GDY catalysts, the electrochemical deposition method, which is easy to operate and environmentally safe, is widely used because it can precisely control the deposition thickness and deposition speed by controlling the process conditions (current, concentration and deposition time) and can be uniformly deposited on a complex substrate. However, it is difficult to prepare materials with complex composition and the doping position and amount of heteroatoms cannot be controlled accurately. The wet chemical method is increasingly frequently used because of its low raw material cost, simple process and easy industrialization, but the low purity and large particle size of the prepared materials are major limitations. In the synthesis of nonmetallic atom-anchored GDY catalysts, the traditional high-temperature annealing synthesis method can better control the doping source and temperature to obtain materials with different structures and doping amounts, but this method usually forms multiple doping sites on the GDY network structure. The preparation method using the Glaser–Hay coupling chemical reaction can controllably synthesize high-purity materials and can precisely control the bonding environment and doping sites, but its operation is difficult and the types of materials that can be synthesized are limited.

In spite of the significant progress that has been made, there are still challenges in theory and practice. The effect of the type of metal atom on the overall catalytic performance and the change of the geometric structure of the active site during the electrocatalytic process require further research efforts. It is indispensable to systematically expand the simple-to-operate and easy-to-implement synthesis method for nonmetallic-atom-doped GDY and to develop other types of nonmetallic-atom-doped GDY catalysts with high-quality catalytic activity. Both the development of nonmetallic-atom-doping or other chemical modification of GDY as the support for metal-atom-anchored catalysts, and the development of a variety of metal-atom-anchored catalysts supported by the functionalized GDY may provide new ideas and open up new fields for the precise design and performance control of multifunctional electrocatalysts in the future.

Additionally, the development of catalysts with ORR and HER catalytic performance comparable to Pt-based catalysts is the current research focus. In addition, the controllable preparation and stability of the catalysts are also issues that require special attention. To date, the OER catalytic performance of many catalysts under alkaline conditions has surpassed that of noble metal catalysts, but catalysts with efficient and stable OER catalysis under acidic conditions still need to be developed. Simultaneously, the development of dual-functional catalysts with stable and high-efficiency HER and OER catalysis and excellent overall water splitting performance is essential to green and renewable energy technologies and has great commercial application prospects. In pursuit of this, more investigations will be needed to deeply explore and understand the chemical and electrochemical properties of GDY, as well as the internal mechanism of function between atoms and GDY and the kinetic and thermodynamic principles of the electrocatalysis process.

**Author Contributions:** X.Q. and J.X. initiated the topic and wrote the draft; Y.Z. and S.C. were involved in the discussion, revision and editing of the Review. J.X. supervised the project. All authors have read and agreed to the published version of the manuscript.

**Funding:** This research was funded by the National Natural Science Foundation of China (Grant Number 21773168), the Fundamental Research Funds for the Central Universities, Nankai Universities (Grant Number 63196009), the research funds of Longyan University (Grant Number LB2018016) and the Young and Middle-aged Teacher in Science Research of Fujian Province (Grant Number No. JAT190732).

**Conflicts of Interest:** The authors declare no conflict of interest.

## References

1. Rod, B.; Jeremy, M.; Bryan, P.; Seung, K.Y.; Rangachary, M.; Nancy, G.; Deborah, M.; Mahlon, W.; Fernando, G.; David, W.; et al. Scientific aspects of polymer electrolyte fuel cell durability and degradation. *Chem. Rev.* **2007**, *107*, 3904–3951. [[CrossRef](#)]

2. Walter, M.G.; Warren, E.L.; McKone, J.R.; Boettcher, S.W.; Mi, Q.; Santori, E.A.; Lewis, N.S. Solar water splitting cells. *Chem. Rev.* **2010**, *110*, 6446–6473. [[CrossRef](#)]
3. Budischak, C.; Sewell, D.; Thomson, H.; Mach, L.; Veron, D.E.; Kempton, W. Cost-minimized combinations of wind power, solar power and electrochemical storage, powering the grid up to 99.9% of the time. *J. Power Sources* **2013**, *225*, 60–74. [[CrossRef](#)]
4. Cook, T.R.; Dogutan, D.K.; Reece, S.Y.; Surendranath, Y.; Teets, T.S.; Nocera, D.G. Solar energy supply and storage for the legacy and nonlegacy worlds. *Chem. Rev.* **2010**, *110*, 6474–6502. [[CrossRef](#)] [[PubMed](#)]
5. Seh, Z.W.; Kibsgaard, J.; Dickens, C.F.; Chorkendorff, I.; Nørskov, J.K.; Jaramillo, T.F. Combining theory and experiment in electrocatalysis: Insights into materials design. *Science* **2017**, *355*. [[CrossRef](#)] [[PubMed](#)]
6. Faber, M.S.; Jin, S. Earth-abundant inorganic electrocatalysts and their nanostructures for energy conversion applications. *Energy Environ. Sci.* **2014**, *7*, 3519–3542. [[CrossRef](#)]
7. McKone, J.R.; Marinescu, S.C.; Brunschwig, B.S.; Winkler, J.R.; Gray, H.B. Earth-abundant hydrogen evolution electrocatalysts. *Chem. Sci.* **2014**, *5*, 865–878. [[CrossRef](#)]
8. Dau, H.; Limberg, C.; Reier, T.; Risch, M.; Roggan, S.; Strasser, P. The Mechanism of Water Oxidation: From Electrolysis via Homogeneous to Biological Catalysis. *ChemCatChem* **2010**, *2*, 724–761. [[CrossRef](#)]
9. Wang, T.; Xie, H.; Chen, M.; D'Aloia, A.; Cho, J.; Wu, G.; Li, Q. Precious metal-free approach to hydrogen electrocatalysis for energy conversion: From mechanism understanding to catalyst design. *Nano Energy* **2017**, *42*, 69–89. [[CrossRef](#)]
10. Sathiskumar, C.; Ramakrishnan, S.; Vinothkannan, M.; Kim, A.R.; Karthikeyan, S.; Yoo, D.J. Nitrogen-Doped Porous Carbon Derived from Biomass Used as Trifunctional Electrocatalyst toward Oxygen Reduction, Oxygen Evolution and Hydrogen Evolution Reactions. *Nanomaterials* **2020**, *10*, 76. [[CrossRef](#)]
11. Elayappan, V.; Shanmugam, R.; Chinnusamy, S.; Yoo, D.J.; Mayakrishnan, G.; Kim, K.; Noh, H.S.; Kim, M.K.; Lee, H. Three-dimensional bimetal TMO supported carbon based electrocatalyst developed via dry synthesis for hydrogen and oxygen evolution. *Appl. Surf. Sci.* **2020**, *505*. [[CrossRef](#)]
12. Zhang, J.; Vukmirovic, M.B.; Sasaki, K.; Nilekar, A.U.; Mavrikakis, M.; Adzic, R.R. Mixed-metal Pt monolayer electrocatalysts for enhanced oxygen reduction kinetics. *J. Am. Chem. Soc.* **2005**, *127*, 12480–12481. [[CrossRef](#)] [[PubMed](#)]
13. Sasaki, K.; Naohara, H.; Choi, Y.; Cai, Y.; Chen, W.F.; Liu, P.; Adzic, R.R. Highly stable Pt monolayer on PdAu nanoparticle electrocatalysts for the oxygen reduction reaction. *Nat. Commun.* **2012**, *3*, 1115. [[CrossRef](#)] [[PubMed](#)]
14. Debe, M.K. Electrocatalyst approaches and challenges for automotive fuel cells. *Nature* **2012**, *486*, 43–51. [[CrossRef](#)]
15. Subbaraman, R.; Tripkovic, D.; Chang, K.-C.; Strmcnik, D.; Paulikas, A.P.; Hirunsit, P.; Chan, M.; Greeley, J.; Stamenkovic, V.; Markovic, N.M. Trends in activity for the water electrolyser reactions on 3d M (Ni,Co,Fe,Mn) hydr (oxy) oxide catalysts. *Nat. Mater.* **2012**, *11*, 550–557. [[CrossRef](#)] [[PubMed](#)]
16. Coleman, J.N.; Lotya, M.; O'Neill, A.; Bergin, S.D.; King, P.J.; Khan, U.; Young, K.; Gaucher, A.; De, S.; Smith, R.J. Two-dimensional nanosheets produced by liquid exfoliation of layered materials. *Science* **2011**, *331*, 568–571. [[CrossRef](#)]
17. Siringhaus, H.; Brown, P.; Friend, R.; Nielsen, M.M.; Bechgaard, K.; Langeveld-Voss, B.; Spiering, A.; Janssen, R.A.; Meijer, E.; Herwig, P. Two-dimensional charge transport in self-organized, high-mobility conjugated polymers. *Nature* **1999**, *401*, 685–688. [[CrossRef](#)]
18. Mortazavi, B.; Makaremi, M.; Shahrokhi, M.; Fan, Z.; Rabczuk, T. N-graphdiyne two-dimensional nanomaterials: Semiconductors with low thermal conductivity and high stretchability. *Carbon* **2018**, *137*, 57–67. [[CrossRef](#)]
19. Shang, H.; Zuo, Z.; Li, L.; Wang, F.; Liu, H.; Li, Y.; Li, Y. Ultrathin Graphdiyne Nanosheets Grown In Situ on Copper Nanowires and Their Performance as Lithium-Ion Battery Anodes. *Angew. Chem. Int. Ed.* **2018**, *57*, 774–778. [[CrossRef](#)]
20. Wang, N.; Li, X.; Tu, Z.; Zhao, F.; He, J.; Guan, Z.; Huang, C.; Yi, Y.; Li, Y. Synthesis and Electronic Structure of Boron-Graphdiyne with an sp-Hybridized Carbon Skeleton and Its Application in Sodium Storage. *Angew. Chem. Int. Ed.* **2018**, *57*, 3968–3973. [[CrossRef](#)]
21. Yang, Z.; Shen, X.; Wang, N.; He, J.; Li, X.; Wang, X.; Hou, Z.; Wang, K.; Gao, J.; Jiu, T.; et al. Graphdiyne Containing Atomically Precise N Atoms for Efficient Anchoring of Lithium Ion. *ACS Appl. Mater. Interfaces* **2019**, *11*, 2608–2617. [[CrossRef](#)] [[PubMed](#)]

22. Rao, C.N.; Sood, A.K.; Subrahmanyam, K.S.; Govindaraj, A. Graphene: The new two-dimensional nanomaterial. *Angew. Chem. Int. Ed.* **2009**, *48*, 7752–7777. [[CrossRef](#)] [[PubMed](#)]
23. Bonaccorso, F.; Colombo, L.; Yu, G.; Stoller, M.; Tozzini, V.; Ferrari, A.C.; Ruoff, R.S.; Pellegrini, V. Graphene, related two-dimensional crystals, and hybrid systems for energy conversion and storage. *Science* **2015**, *347*, 1246501. [[CrossRef](#)] [[PubMed](#)]
24. Thomas, A.; Fischer, A.; Goettmann, F.; Antonietti, M.; Müller, J.-O.; Schlögl, R.; Carlsson, J.M. Graphitic carbon nitride materials: Variation of structure and morphology and their use as metal-free catalysts. *J. Mater. Chem.* **2008**, *18*, 4893–4908. [[CrossRef](#)]
25. Wang, X.; Chen, X.; Thomas, A.; Fu, X.; Antonietti, M. Metal-Containing Carbon Nitride Compounds: A New Functional Organic-Metal Hybrid Material. *Adv. Mater.* **2009**, *21*, 1609–1612. [[CrossRef](#)]
26. Li, G.; Li, Y.; Liu, H.; Guo, Y.; Li, Y.; Zhu, D. Architecture of graphdiyne nanoscale films. *Chem. Commun.* **2010**, *46*, 3256–3258. [[CrossRef](#)]
27. Matsuoka, R.; Sakamoto, R.; Hoshiko, K.; Sasaki, S.; Masunaga, H.; Nagashio, K.; Nishihara, H. Crystalline Graphdiyne Nanosheets Produced at a Gas/Liquid or Liquid/Liquid Interface. *J. Am. Chem. Soc.* **2017**, *139*, 3145–3152. [[CrossRef](#)]
28. Li, Y.; Xu, L.; Liu, H.; Li, Y. Graphdiyne and graphyne: From theoretical predictions to practical construction. *Chem. Soc. Rev.* **2014**, *43*, 2572–2586. [[CrossRef](#)]
29. Guo, J.; Wang, Z.; Shi, R.; Zhang, Y.; He, Z.; Gao, L.; Wang, R.; Shu, Y.; Ma, C.; Ge, Y.; et al. Graphdiyne as a Promising Mid-Infrared Nonlinear Optical Material for Ultrafast Photonics. *Adv. Opt. Mater.* **2020**, *8*, 2000067. [[CrossRef](#)]
30. Ren, Y.; Dong, Y.; Feng, Y.; Xu, J. Compositing Two-Dimensional Materials with TiO<sub>2</sub> for Photocatalysis. *Catalysts* **2018**, *8*, 590. [[CrossRef](#)]
31. Huang, C.-S.; Li, Y.-L. Structure of 2D Graphdiyne and Its Application in Energy Fields. *Acta Phys. Chim. Sin.* **2016**, *32*, 1314–1329. [[CrossRef](#)]
32. Xue, Z.; Zhu, M.; Dong, Y.; Feng, T.; Chen, Z.; Feng, Y.; Shan, Z.; Xu, J.; Meng, S. An integrated targeting drug delivery system based on the hybridization of graphdiyne and MOFs for visualized cancer therapy. *Nanoscale* **2019**, *11*, 11709–11718. [[CrossRef](#)] [[PubMed](#)]
33. Yu, H.; Xue, Y.; Li, Y. Graphdiyne and its Assembly Architectures: Synthesis, Functionalization, and Applications. *Adv. Mater.* **2019**, *31*, 1803101. [[CrossRef](#)] [[PubMed](#)]
34. Zuo, Z.; Wang, D.; Zhang, J.; Lu, F.; Li, Y. Synthesis and Applications of Graphdiyne-Based Metal-Free Catalysts. *Adv. Mater.* **2019**, *31*, 1803762. [[CrossRef](#)]
35. Qi, H.; Yu, P.; Wang, Y.; Han, G.; Liu, H.; Yi, Y.; Li, Y.; Mao, L. Graphdiyne Oxides as Excellent Substrate for Electroless Deposition of Pd Clusters with High Catalytic Activity. *J. Am. Chem. Soc.* **2015**, *137*, 5260–5263. [[CrossRef](#)]
36. Li, Y.; Guo, C.; Li, J.; Liao, W.; Li, Z.; Zhang, J.; Chen, C. Pyrolysis-induced synthesis of iron and nitrogen-containing carbon nanolayers modified graphdiyne nanostructure as a promising core-shell electrocatalyst for oxygen reduction reaction. *Carbon* **2017**, *119*, 201–210. [[CrossRef](#)]
37. Shi, G.; Yu, C.; Fan, Z.; Li, J.; Yuan, M. Graphdiyne-Supported NiFe Layered Double Hydroxide Nanosheets as Functional Electrocatalysts for Oxygen Evolution. *ACS Appl. Mater. Interfaces* **2019**, *11*, 2662–2669. [[CrossRef](#)]
38. Guo, Y.; Liu, J.; Yang, Q.; Ma, L.; Zhao, Y.; Huang, Z.; Li, X.; Dong, B.; Fu, X.Z.; Zhi, C. Metal-Tuned Acetylene Linkages in Hydrogen Substituted Graphdiyne Boosting the Electrochemical Oxygen Reduction. *Small* **2020**, *16*, 1907341. [[CrossRef](#)]
39. Lv, Q.; Si, W.; He, J.; Sun, L.; Zhang, C.; Wang, N.; Yang, Z.; Li, X.; Wang, X.; Deng, W.; et al. Selectively nitrogen-doped carbon materials as superior metal-free catalysts for oxygen reduction. *Nat. Commun.* **2018**, *9*, 3376. [[CrossRef](#)]
40. Haley, M.M. Synthesis and properties of annulenic subunits of graphyne and graphdiyne nanoarchitectures. *Pure Appl. Chem.* **2008**, *80*, 519–532. [[CrossRef](#)]
41. He, J.; Ma, S.Y.; Zhou, P.; Zhang, C.X.; He, C.; Sun, L.Z. Magnetic Properties of Single Transition-Metal Atom Absorbed Graphdiyne and Graphyne Sheet from DFT+U Calculations. *J. Phys. Chem. C* **2012**, *116*, 26313–26321. [[CrossRef](#)]
42. Zuo, Z.; Li, Y. Emerging Electrochemical Energy Applications of Graphdiyne. *Joule* **2019**, *3*, 899–903. [[CrossRef](#)]

43. Huang, C.; Li, Y.; Wang, N.; Xue, Y.; Zuo, Z.; Liu, H.; Li, Y. Progress in Research into 2D Graphdiyne-Based Materials. *Chem. Rev.* **2018**, *118*, 7744–7803. [[CrossRef](#)] [[PubMed](#)]
44. Liu, R.; Gao, X.; Zhou, J.; Xu, H.; Li, Z.; Zhang, S.; Xie, Z.; Zhang, J.; Liu, Z. Chemical Vapor Deposition Growth of Linked Carbon Monolayers with Acetylenic Scaffoldings on Silver Foil. *Adv. Mater.* **2017**, *29*, 1604665. [[CrossRef](#)]
45. Jiang, X.; Zhao, X.; Bao, W.; Shi, R.; Zhao, J.; Kang, J.; Xia, X.; Chen, H.; Li, H.; Xu, J.; et al. Graphdiyne Nanosheets for Multicolor Random Lasers. *ACS Appl. Nano Mater.* **2020**. [[CrossRef](#)]
46. Zhou, J.; Gao, X.; Liu, R.; Xie, Z.; Yang, J.; Zhang, S.; Zhang, G.; Liu, H.; Li, Y.; Zhang, J.; et al. Synthesis of Graphdiyne Nanowalls Using Acetylenic Coupling Reaction. *J. Am. Chem. Soc.* **2015**, *137*, 7596–7599. [[CrossRef](#)]
47. Li, G.; Li, Y.; Qian, X.; Liu, H.; Lin, H.; Chen, N.; Li, Y. Construction of Tubular Molecule Aggregations of Graphdiyne for Highly Efficient Field Emission. *J. Phys. Chem. C* **2011**, *115*, 2611–2615. [[CrossRef](#)]
48. Zuo, Z.; Shang, H.; Chen, Y.; Li, J.; Liu, H.; Li, Y.; Li, Y. A facile approach for graphdiyne preparation under atmosphere for an advanced battery anode. *Chem. Commun.* **2017**, *53*, 8074–8077. [[CrossRef](#)]
49. Gao, X.; Ren, H.; Zhou, J.; Du, R.; Yin, C.; Liu, R.; Peng, H.; Tong, L.; Liu, Z.; Zhang, J. Synthesis of Hierarchical Graphdiyne-Based Architecture for Efficient Solar Steam Generation. *Chem. Mater.* **2017**, *29*, 5777–5781. [[CrossRef](#)]
50. Cirera, B.; Zhang, Y.Q.; Bjork, J.; Klyatskaya, S.; Chen, Z.; Ruben, M.; Barth, J.V.; Klappenberger, F. Synthesis of extended graphdiyne wires by vicinal surface templating. *Nano Lett.* **2014**, *14*, 1891–1897. [[CrossRef](#)]
51. Wu, L.; Dong, Y.; Zhao, J.; Ma, D.; Huang, W.; Zhang, Y.; Wang, Y.; Jiang, X.; Xiang, Y.; Li, J.; et al. Kerr Nonlinearity in 2D Graphdiyne for Passive Photonic Diodes. *Adv. Mater.* **2019**, *31*, 1807981. [[CrossRef](#)] [[PubMed](#)]
52. Dong, Y.; Semin, S.; Feng, Y.; Xu, J.; Rasing, T. Solvent induced enhancement of nonlinear optical response of graphdiyne. *Chin. Chem. Lett.* **2020**. [[CrossRef](#)]
53. Jia, Z.; Li, Y.; Zuo, Z.; Liu, H.; Huang, C.; Li, Y. Synthesis and Properties of 2D Carbon—Graphdiyne. *Acc. Chem. Res.* **2017**, *50*, 2470–2478. [[CrossRef](#)] [[PubMed](#)]
54. Fei, H.; Dong, J.; Feng, Y.; Allen, C.S.; Wan, C.; Voloskiy, B.; Li, M.; Zhao, Z.; Wang, Y.; Sun, H. General synthesis and definitive structural identification of  $\text{MN}_4\text{C}_4$  single-atom catalysts with tunable electrocatalytic activities. *Nat. Catal.* **2018**, *1*, 63–72. [[CrossRef](#)]
55. Jones, J.; Xiong, H.; DeLaRiva, A.T.; Peterson, E.J.; Pham, H.; Challa, S.R.; Qi, G.; Oh, S.; Wiebenga, M.H.; Hernandez, X.I.P.; et al. Thermally stable single-atom platinum-on-ceria catalysts via atom trapping. *Sciences* **2016**, *353*, 150–154. [[CrossRef](#)]
56. Thomas, J.M. Catalysis: Tens of thousands of atoms replaced by one. *Nature* **2015**, *525*, 325–326. [[CrossRef](#)]
57. Lin, Z.-Z. Graphdiyne as a promising substrate for stabilizing Pt nanoparticle catalyst. *Carbon* **2015**, *86*, 301–309. [[CrossRef](#)]
58. Ma, D.W.; Li, T.; Wang, Q.; Yang, G.; He, C.; Ma, B.; Lu, Z. Graphyne as a promising substrate for the noble-metal single-atom catalysts. *Carbon* **2015**, *95*, 756–765. [[CrossRef](#)]
59. Li, J.; Gao, X.; Jiang, X.; Li, X.-B.; Liu, Z.; Zhang, J.; Tung, C.-H.; Wu, L.-Z. Graphdiyne: A Promising Catalyst-Support To Stabilize Cobalt Nanoparticles for Oxygen Evolution. *ACS Catal.* **2017**, *7*, 5209–5213. [[CrossRef](#)]
60. Mashhadzadeh, A.H.; Vahedi, A.M.; Ardjmand, M.; Ahangari, M.G. Investigation of heavy metal atoms adsorption onto graphene and graphdiyne surface: A density functional theory study. *Superlattices Microstruct.* **2016**, *100*, 1094–1102. [[CrossRef](#)]
61. Lin, J.; Qiao, B.; Li, N.; Li, L.; Sun, X.; Liu, J.; Wang, X.; Zhang, T. Little do more: A highly effective  $\text{Pt}_{(1)}/\text{FeO}(x)$  single-atom catalyst for the reduction of NO by  $\text{H}_2$ . *Chem. Commun.* **2015**, *51*, 7911–7914. [[CrossRef](#)] [[PubMed](#)]
62. Yin, X.P.; Wang, H.J.; Tang, S.F.; Lu, X.L.; Shu, M.; Si, R.; Lu, T.B. Engineering the Coordination Environment of Single-Atom Platinum Anchored on Graphdiyne for Optimizing Electrocatalytic Hydrogen Evolution. *Angew. Chem. Int. Ed.* **2018**, *57*, 9382–9386. [[CrossRef](#)] [[PubMed](#)]
63. Hui, L.; Xue, Y.; Yu, H.; Liu, Y.; Fang, Y.; Xing, C.; Huang, B.; Li, Y. Highly Efficient and Selective Generation of Ammonia and Hydrogen on a Graphdiyne-Based Catalyst. *J. Am. Chem. Soc.* **2019**, *141*, 10677–10683. [[CrossRef](#)] [[PubMed](#)]

64. Yu, H.; Hui, L.; Xue, Y.; Liu, Y.; Fang, Y.; Xing, C.; Zhang, C.; Zhang, D.; Chen, X.; Du, Y.; et al. 2D graphdiyne loading ruthenium atoms for high efficiency water splitting. *Nano Energy* **2020**, *72*, 104667. [[CrossRef](#)]
65. McKeown, D.A.; Hagans, P.L.; Carette, L.P.; Russell, A.E.; Swider, K.E.; Rolison, D.R. Structure of hydrous ruthenium oxides: Implications for charge storage. *J. Phys. Chem. B* **1999**, *103*, 4825–4832. [[CrossRef](#)]
66. Ribeiro, J.; Tremiliosi-Filho, G.; Olivi, P.; de Andrade, A.R. XAS characterization of the RuO<sub>2</sub>-Ta<sub>2</sub>O<sub>5</sub> system local (crystal) structure. *Mater. Chem. Phys.* **2011**, *125*, 449–460. [[CrossRef](#)]
67. Xue, Y.; Huang, B.; Yi, Y.; Guo, Y.; Zuo, Z.; Li, Y.; Jia, Z.; Liu, H.; Li, Y. Anchoring zero valence single atoms of nickel and iron on graphdiyne for hydrogen evolution. *Nat. Commun.* **2018**, *9*, 1460. [[CrossRef](#)]
68. Yu, H.; Xue, Y.; Huang, B.; Hui, L.; Zhang, C.; Fang, Y.; Liu, Y.; Zhao, Y.; Li, Y.; Liu, H.; et al. Ultrathin Nanosheet of Graphdiyne-Supported Palladium Atom Catalyst for Efficient Hydrogen Production. *IScience* **2019**, *11*, 31–41. [[CrossRef](#)]
69. Xue, Y.; Li, Y.; Zhang, J.; Liu, Z.; Zhao, Y. 2D graphdiyne materials: Challenges and opportunities in energy field. *Sci. China Chem.* **2018**, *61*, 765–786. [[CrossRef](#)]
70. Wei, D.; Liu, Y.; Wang, Y.; Zhang, H.; Huang, L.; Yu, G. Synthesis of N-doped graphene by chemical vapor deposition and its electrical properties. *Nano Lett.* **2009**, *9*, 1752–1758. [[CrossRef](#)]
71. Luo, Z.; Lim, S.; Tian, Z.; Shang, J.; Lai, L.; MacDonald, B.; Fu, C.; Shen, Z.; Yu, T.; Lin, J. Pyridinic N doped graphene: Synthesis, electronic structure, and electrocatalytic property. *J. Mater. Chem.* **2011**, *21*, 8038–8044. [[CrossRef](#)]
72. Qu, L.; Liu, Y.; Baek, J.-B.; Dai, L. Nitrogen-doped graphene as efficient metal-free electrocatalyst for oxygen reduction in fuel cells. *ACS Nano* **2010**, *4*, 1321–1326. [[CrossRef](#)]
73. Zhang, C.; Fu, L.; Liu, N.; Liu, M.; Wang, Y.; Liu, Z. Synthesis of nitrogen-doped graphene using embedded carbon and nitrogen sources. *Adv. Mater.* **2011**, *23*, 1020–1024. [[CrossRef](#)] [[PubMed](#)]
74. Deng, D.; Pan, X.; Yu, L.; Cui, Y.; Jiang, Y.; Qi, J.; Li, W.-X.; Fu, Q.; Ma, X.; Xue, Q.; et al. Toward N-Doped Graphene via Solvothermal Synthesis. *Chem. Mater.* **2011**, *23*, 1188–1193. [[CrossRef](#)]
75. Ghosh, A.; Late, D.J.; Panchakarla, L.S.; Govindaraj, A.; Rao, C.N.R. NO<sub>2</sub> and humidity sensing characteristics of few-layer graphenes. *J. Exp. Nanosci.* **2009**, *4*, 313–322. [[CrossRef](#)]
76. Chipeng, X.; Ning, W.; Xiaofang, L.; Guorong, X.; Changshui, H. Research on the Preparation of Graphdiyne and Its Derivatives. *Chemistry* **2020**, *26*, 569–583. [[CrossRef](#)]
77. Yang, Z.; Cui, W.; Wang, K.; Song, Y.; Zhao, F.; Wang, N.; Long, Y.; Wang, H.; Huang, C. Chemical Modification of the sp-Hybridized Carbon Atoms of Graphdiyne by Using Organic Sulfur. *Chemistry* **2019**, *25*, 5643–5647. [[CrossRef](#)]
78. Zhao, Y.; Yang, N.; Yao, H.; Liu, D.; Song, L.; Zhu, J.; Li, S.; Gu, L.; Lin, K.; Wang, D. Stereodefined Codoping of sp-N and S Atoms in Few-Layer Graphdiyne for Oxygen Evolution Reaction. *J. Am. Chem. Soc.* **2019**, *141*, 7240–7244. [[CrossRef](#)]
79. Zhang, S.; Cai, Y.; He, H.; Zhang, Y.; Liu, R.; Cao, H.; Wang, M.; Liu, J.; Zhang, G.; Li, Y.; et al. Heteroatom doped graphdiyne as efficient metal-free electrocatalyst for oxygen reduction reaction in alkaline medium. *J. Mater. Chem. A* **2016**, *4*, 4738–4744. [[CrossRef](#)]
80. Zou, H.; Rong, W.; Long, B.; Ji, Y.; Duan, L. Corrosion-Induced Cl-Doped Ultrathin Graphdiyne toward Electrocatalytic Nitrogen Reduction at Ambient Conditions. *ACS Catal.* **2019**, *9*, 10649–10655. [[CrossRef](#)]
81. Lv, Q.; Wang, N.; Si, W.; Hou, Z.; Li, X.; Wang, X.; Zhao, F.; Yang, Z.; Zhang, Y.; Huang, C. Pyridinic nitrogen exclusively doped carbon materials as efficient oxygen reduction electrocatalysts for Zn-air batteries. *Appl. Catal. B* **2020**, *261*, 118234. [[CrossRef](#)]
82. Zhao, Y.; Wan, J.; Yao, H.; Zhang, L.; Lin, K.; Wang, L.; Yang, N.; Liu, D.; Song, L.; Zhu, J.; et al. Few-layer graphdiyne doped with sp-hybridized nitrogen atoms at acetylenic sites for oxygen reduction electrocatalysis. *Nat. Chem.* **2018**, *10*, 924–931. [[CrossRef](#)] [[PubMed](#)]
83. Liu, R.; Liu, H.; Li, Y.; Yi, Y.; Shang, X.; Zhang, S.; Yu, X.; Zhang, S.; Cao, H.; Zhang, G. Nitrogen-doped graphdiyne as a metal-free catalyst for high-performance oxygen reduction reactions. *Nanoscale* **2014**, *6*, 11336–11343. [[CrossRef](#)] [[PubMed](#)]
84. Nowicki, P.; Pietrzak, R.; Wachowska, H. X-ray Photoelectron Spectroscopy Study of Nitrogen-Enriched Active Carbons Obtained by Ammoxidation and Chemical Activation of Brown and Bituminous Coals. *Energy Fuels* **2010**, *24*, 1197–1206. [[CrossRef](#)]
85. Pietrzak, R. XPS study and physico-chemical properties of nitrogen-enriched microporous activated carbon from high volatile bituminous coal. *Fuel* **2009**, *88*, 1871–1877. [[CrossRef](#)]

86. Estrade-Szwarczkopf, H. XPS photoemission in carbonaceous materials: A “defect” peak beside the graphitic asymmetric peak. *Carbon* **2004**, *42*, 1713–1721. [[CrossRef](#)]
87. Ihm, K.; Kang, T.-H.; Lee, D.H.; Park, S.-Y.; Kim, K.-J.; Kim, B.; Yang, J.H.; Park, C.Y. Oxygen contaminants affecting on the electronic structures of the carbon nano tubes grown by rapid thermal chemical vapor deposition. *Surf. Sci.* **2006**, *600*, 3729–3733. [[CrossRef](#)]
88. Xue, Q.; Ding, Y.; Xue, Y.; Li, F.; Chen, P.; Chen, Y. 3D nitrogen-doped graphene aerogels as efficient electrocatalyst for the oxygen reduction reaction. *Carbon* **2018**, *139*, 137–144. [[CrossRef](#)]
89. Fei, H.; Dong, J.; Arellano-Jimenez, M.J.; Ye, G.; Dong Kim, N.; Samuel, E.L.; Peng, Z.; Zhu, Z.; Qin, F.; Bao, J.; et al. Atomic cobalt on nitrogen-doped graphene for hydrogen generation. *Nat. Commun.* **2015**, *6*, 8668. [[CrossRef](#)]
90. Zhou, S.; Liu, N.; Wang, Z.; Zhao, J. Nitrogen-Doped Graphene on Transition Metal Substrates as Efficient Bifunctional Catalysts for Oxygen Reduction and Oxygen Evolution Reactions. *ACS Appl. Mater. Interfaces* **2017**, *9*, 22578–22587. [[CrossRef](#)]
91. Bayatsarmadi, B.; Zheng, Y.; Vasileff, A.; Qiao, S.Z. Recent Advances in Atomic Metal Doping of Carbon-based Nanomaterials for Energy Conversion. *Small* **2017**, *13*, 1700191. [[CrossRef](#)] [[PubMed](#)]
92. Wu, P.; Du, P.; Zhang, H.; Cai, C. Graphdiyne as a metal-free catalyst for low-temperature CO oxidation. *Phys. Chem. Chem. Phys.* **2014**, *16*, 5640–5648. [[CrossRef](#)] [[PubMed](#)]
93. Lu, Z.; Li, S.; Lv, P.; He, C.; Ma, D.; Yang, Z. First principles study on the interfacial properties of NM/graphdiyne (NM = Pd, Pt, Rh and Ir): The implications for NM growing. *Appl. Surf. Sci.* **2016**, *360*, 1–7. [[CrossRef](#)]
94. Sun, M.; Wu, T.; Xue, Y.; Dougherty, A.W.; Huang, B.; Li, Y.; Yan, C.-H. Mapping of atomic catalyst on graphdiyne. *Nano Energy* **2019**, *62*, 754–763. [[CrossRef](#)]
95. Feng, Z.; Li, R.; Ma, Y.; Li, Y.; Wei, D.; Tang, Y.; Dai, X. Molecule-level graphdiyne coordinated transition metals as a new class of bifunctional electrocatalysts for oxygen reduction and oxygen evolution reactions. *Phys. Chem. Chem. Phys.* **2019**, *21*, 19651–19659. [[CrossRef](#)]
96. Nørskov, J.K.; Rossmeisl, J.; Logadottir, A.; Lindqvist, L.; Kitchin, J.R.; Bligaard, T.; Jónsson, H. Origin of the Overpotential for Oxygen Reduction at a Fuel-Cell Cathode. *J. Phys. Chem. B* **2004**, *108*, 17886–17892. [[CrossRef](#)]
97. Cheng, C.; Zhang, X.; Fu, Z.; Yang, Z. Strong metal-support interactions impart activity in the oxygen reduction reaction: Au monolayer on Mo<sub>2</sub>C (MXene). *J. Phys. Condens. Matter* **2018**, *30*, 475201. [[CrossRef](#)]
98. Bashyam, R.; Zelenay, P. A class of non-precious metal composite catalysts for fuel cells. *Nature* **2006**, *443*, 63–66. [[CrossRef](#)]
99. Geng, D.; Chen, Y.; Chen, Y.; Li, Y.; Li, R.; Sun, X.; Ye, S.; Knights, S. High oxygen-reduction activity and durability of nitrogen-doped graphene. *Energy Environ. Sci.* **2011**, *4*, 760–764. [[CrossRef](#)]
100. Liu, X.; Li, L.; Meng, C.; Han, Y. Palladium Nanoparticles/Defective Graphene Composites as Oxygen Reduction Electrocatalysts: A First-Principles Study. *J. Phys. Chem. C* **2012**, *116*, 2710–2719. [[CrossRef](#)]
101. Wang, H.; Maiyalagan, T.; Wang, X. Review on Recent Progress in Nitrogen-Doped Graphene: Synthesis, Characterization, and Its Potential Applications. *ACS Catal.* **2012**, *2*, 781–794. [[CrossRef](#)]
102. Wang, S.; Yu, D.; Dai, L. Polyelectrolyte functionalized carbon nanotubes as efficient metal-free electrocatalysts for oxygen reduction. *J. Am. Chem. Soc.* **2011**, *133*, 5182–5185. [[CrossRef](#)] [[PubMed](#)]
103. Maldonado, S.; Stevenson, K.J. Influence of Nitrogen Doping on Oxygen Reduction Electrocatalysis at Carbon Nanofiber Electrodes. *J. Phys. Chem. B* **2005**, *109*, 4707–4716. [[CrossRef](#)] [[PubMed](#)]
104. Feng, Z.; Ma, Y.; Li, Y.; Li, R.; Liu, J.; Li, H.; Tang, Y.; Dai, X. Graphdiyne doped with sp-hybridized nitrogen atoms at acetylenic sites as potential metal-free electrocatalysts for oxygen reduction reaction. *J. Phys. Condens. Matter* **2019**, *31*, 465201. [[CrossRef](#)]
105. Feng, Z.; Ma, Y.; Li, Y.; Li, R.; Tang, Y.; Dai, X. Charge-compensated co-doping of graphdiyne with boron and nitrogen to form metal-free electrocatalysts for the oxygen reduction reaction. *Phys. Chem. Chem. Phys.* **2020**, *22*, 1493–1501. [[CrossRef](#)]
106. Kang, B.; Wu, S.; Ma, J.; Ai, H.; Lee, J.Y. Synergy of sp-N and sp<sup>2</sup>-N codoping endows graphdiyne with comparable oxygen reduction reaction performance to Pt. *Nanoscale* **2019**, *11*, 16599–16605. [[CrossRef](#)]
107. Gu, J.; Magagula, S.; Zhao, J.; Chen, Z. Boosting ORR/OER Activity of Graphdiyne by Simple Heteroatom Doping. *Small Methods* **2019**, *3*, 1800550. [[CrossRef](#)]

108. Chen, X.; Ong, W.-J.; Kong, Z.; Zhao, X.; Li, N. Probing the active sites of site-specific nitrogen doping in metal-free graphdiyne for electrochemical oxygen reduction reactions. *Sci. Bull.* **2020**, *65*, 45–54. [[CrossRef](#)]
109. Das, B.K.; Sen, D.; Chattopadhyay, K.K. Implications of boron doping on electrocatalytic activities of graphyne and graphdiyne families: A first principles study. *Phys. Chem. Chem. Phys.* **2016**, *18*, 2949–2958. [[CrossRef](#)]
110. Ketabi, N.; Tolhurst, T.M.; Leedahl, B.; Liu, H.; Li, Y.; Moewes, A. How functional groups change the electronic structure of graphdiyne: Theory and experiment. *Carbon* **2017**, *123*, 1–6. [[CrossRef](#)]
111. Das, B.K.; Sen, D.; Chattopadhyay, K.K. Nitrogen doping in acetylene bonded two dimensional carbon crystals: Ab-initio forecast of electrocatalytic activities vis-à-vis boron doping. *Carbon* **2016**, *105*, 330–339. [[CrossRef](#)]
112. Ren, H.; Shao, H.; Zhang, L.; Guo, D.; Jin, Q.; Yu, R.; Wang, L.; Li, Y.; Wang, Y.; Zhao, H.; et al. A New Graphdiyne Nanosheet/Pt Nanoparticle-Based Counter Electrode Material with Enhanced Catalytic Activity for Dye-Sensitized Solar Cells. *Adv. Energy Mater.* **2015**, *5*, 1500296. [[CrossRef](#)]
113. Kondori, A.; Esmailirad, M.; Baskin, A.; Song, B.; Wei, J.; Chen, W.; Segre, C.U.; Shahbazian-Yassar, R.; Prendergast, D.; Asadi, M. Identifying Catalytic Active Sites of Trimolybdenum Phosphide (Mo<sub>3</sub>P) for Electrochemical Hydrogen Evolution. *Adv. Energy Mater.* **2019**, *9*, 1900516. [[CrossRef](#)]
114. Sun, H.; Yan, Z.; Liu, F.; Xu, W.; Cheng, F.; Chen, J. Self-Supported Transition-Metal-Based Electrocatalysts for Hydrogen and Oxygen Evolution. *Adv. Mater.* **2020**, *32*, 1806326. [[CrossRef](#)] [[PubMed](#)]
115. Cheng, N.; Stambula, S.; Wang, D.; Banis, M.N.; Liu, J.; Riese, A.; Xiao, B.; Li, R.; Sham, T.K.; Liu, L.M.; et al. Platinum single-atom and cluster catalysis of the hydrogen evolution reaction. *Nat. Commun.* **2016**, *7*, 13638. [[CrossRef](#)] [[PubMed](#)]
116. Zheng, Y.; Jiao, Y.; Li, L.H.; Xing, T.; Chen, Y.; Jaroniec, M.; Qiao, S.Z. Toward Design of Synergistically Active Carbon-Based Catalysts for Electrocatalytic Hydrogen Evolution. *ACS Nano* **2014**, *8*, 5290–5296. [[CrossRef](#)]
117. Zheng, Y.; Jiao, Y.; Zhu, Y.; Li, L.H.; Han, Y.; Chen, Y.; Du, A.; Jaroniec, M.; Qiao, S.Z. Hydrogen evolution by a metal-free electrocatalyst. *Nat. Commun.* **2014**, *5*, 3783. [[CrossRef](#)]
118. Qiu, H.J.; Ito, Y.; Cong, W.; Tan, Y.; Liu, P.; Hirata, A.; Fujita, T.; Tang, Z.; Chen, M. Nanoporous Graphene with Single-Atom Nickel Dopants: An Efficient and Stable Catalyst for Electrochemical Hydrogen Production. *Angew. Chem. Int. Ed.* **2015**, *54*, 14031–14035. [[CrossRef](#)]
119. Sun, M.; Dougherty, A.W.; Huang, B.; Li, Y.; Yan, C.H. Accelerating Atomic Catalyst Discovery by Theoretical Calculations-Machine Learning Strategy. *Adv. Energy Mater.* **2020**, *10*, 1903949. [[CrossRef](#)]
120. Guo, J.; Shi, R.; Wang, R.; Wang, Y.; Zhang, F.; Wang, C.; Chen, H.; Ma, C.; Wang, Z.; Ge, Y.; et al. Graphdiyne-Polymer Nanocomposite as a Broadband and Robust Saturable Absorber for Ultrafast Photonics. *Laser Photonics Rev.* **2020**, *14*, 1900367. [[CrossRef](#)]
121. Zhang, Y.; Huang, P.; Guo, J.; Shi, R.; Huang, W.; Shi, Z.; Wu, L.; Zhang, F.; Gao, L.; Li, C.; et al. Graphdiyne-Based Flexible Photodetectors with High Responsivity and Detectivity. *Adv. Mater.* **2020**. [[CrossRef](#)] [[PubMed](#)]
122. Sun, L.; Jiang, P.H.; Liu, H.J.; Fan, D.D.; Liang, J.H.; Wei, J.; Cheng, L.; Zhang, J.; Shi, J. Graphdiyne: A two-dimensional thermoelectric material with high figure of merit. *Carbon* **2015**, *90*, 255–259. [[CrossRef](#)]
123. He, T.; Matta, S.K.; Will, G.; Du, A. Transition-Metal Single Atoms Anchored on Graphdiyne as High-Efficiency Electrocatalysts for Water Splitting and Oxygen Reduction. *Small Methods* **2019**, *3*, 1800419. [[CrossRef](#)]
124. Li, Y.; Li, Y.; Zhu, E.; McLouth, T.; Chiu, C.Y.; Huang, X.; Huang, Y. Stabilization of high-performance oxygen reduction reaction Pt electrocatalyst supported on reduced graphene oxide/carbon black composite. *J. Am. Chem. Soc.* **2012**, *134*, 12326–12329. [[CrossRef](#)]
125. Zhu, H.; Zhang, S.; Guo, S.; Su, D.; Sun, S. Synthetic control of FePtM nanorods (M = Cu, Ni) to enhance the oxygen reduction reaction. *J. Am. Chem. Soc.* **2013**, *135*, 7130–7133. [[CrossRef](#)]
126. Li, H.-H.; Ma, S.-Y.; Fu, Q.-Q.; Liu, X.-J.; Wu, L.; Yu, S.-H. Scalable Bromide-Triggered Synthesis of Pd@Pt Core-Shell Ultrathin Nanowires with Enhanced Electrocatalytic Performance toward Oxygen Reduction Reaction. *J. Am. Chem. Soc.* **2015**, *137*, 7862–7868. [[CrossRef](#)]
127. Nie, Y.; Li, L.; Wei, Z. Recent advancements in Pt and Pt-free catalysts for oxygen reduction reaction. *Chem. Soc. Rev.* **2015**, *44*, 2168–2201. [[CrossRef](#)]
128. Xia, W.; Mahmood, A.; Liang, Z.; Zou, R.; Guo, S. Earth-Abundant Nanomaterials for Oxygen Reduction. *Angew. Chem. Int. Ed.* **2016**, *55*, 2650–2676. [[CrossRef](#)]
129. Su, J.; Ge, R.; Dong, Y.; Hao, F.; Chen, L. Recent progress in single-atom electrocatalysts: Concept, synthesis, and applications in clean energy conversion. *J. Mater. Chem. A* **2018**, *6*, 14025–14042. [[CrossRef](#)]

130. Alarawi, A.; Ramalingam, V.; He, J.-H. Recent advances in emerging single atom confined two-dimensional materials for water splitting applications. *Mater. Today Energy* **2019**, *11*, 1–23. [[CrossRef](#)]
131. Chen, Z.W.; Chen, L.X.; Yang, C.C.; Jiang, Q. Atomic (single, double, and triple atoms) catalysis: Frontiers, opportunities, and challenges. *J. Mater. Chem. A* **2019**, *7*, 3492–3515. [[CrossRef](#)]
132. Xiao-Feng, Y.; Ai Qin, W.; Botao, Q.; Jun, L.; Jingyue, L.; Tao, Z. Single-atom catalysts: A new frontier in heterogeneous catalysis. *Acc. Chem. Res.* **2013**, *46*, 1740–1748. [[CrossRef](#)]
133. Su, D.S.; Perathoner, S.; Centi, G. Nanocarbons for the development of advanced catalysts. *Chem. Rev.* **2013**, *113*, 5782–5816. [[CrossRef](#)] [[PubMed](#)]
134. Ramakrishnan, S.; Karuppannan, M.; Vinothkannan, M.; Ramachandran, K.; Kwon, O.J.; Yoo, D.J. Ultrafine Pt Nanoparticles Stabilized by MoS<sub>2</sub>/N-Doped Reduced Graphene Oxide as a Durable Electrocatalyst for Alcohol Oxidation and Oxygen Reduction Reactions. *ACS Appl. Mater. Interfaces* **2019**, *11*, 12504–12515. [[CrossRef](#)]
135. Gao, Y.; Cai, Z.; Wu, X.; Lv, Z.; Wu, P.; Cai, C. Graphdiyne-Supported Single-Atom-Sized Fe Catalysts for the Oxygen Reduction Reaction: DFT Predictions and Experimental Validations. *ACS Catal.* **2018**, *8*, 10364–10374. [[CrossRef](#)]
136. Wang, M.-Q.; Yang, W.-H.; Wang, H.-H.; Chen, C.; Zhou, Z.-Y.; Sun, S.-G. Pyrolyzed Fe–N–C Composite as an Efficient Non-precious Metal Catalyst for Oxygen Reduction Reaction in Acidic Medium. *ACS Catal.* **2014**, *4*, 3928–3936. [[CrossRef](#)]
137. Kibsgaard, J.; Jaramillo, T.F.; Besenbacher, F. Building an appropriate active-site motif into a hydrogen-evolution catalyst with thiomolybdate [Mo<sub>3</sub>S<sub>13</sub>]<sup>2-</sup> clusters. *Nat. Chem.* **2014**, *6*, 248–253. [[CrossRef](#)]
138. Popczun, E.J.; McKone, J.R.; Read, C.G.; Biacchi, A.J.; Wiltrout, A.M.; Lewis, N.S.; Schaak, R.E. Nanostructured nickel phosphide as an electrocatalyst for the hydrogen evolution reaction. *J. Am. Chem. Soc.* **2013**, *135*, 9267–9270. [[CrossRef](#)]
139. Shi, G.; Xie, Y.; Du, L.; Fan, Z.; Chen, X.; Fu, X.; Xie, W.; Wang, M.; Yuan, M. Stabilization of cobalt clusters with graphdiyne enabling efficient overall water splitting. *Nano Energy* **2020**, *74*, 104852. [[CrossRef](#)]
140. Zhang, J.; Chen, G.; Mullen, K.; Feng, X. Carbon-Rich Nanomaterials: Fascinating Hydrogen and Oxygen Electrocatalysts. *Adv. Mater.* **2018**, *30*, 1800528. [[CrossRef](#)]
141. Wang, Y.; Yang, P.; Zheng, L.; Shi, X.; Zheng, H. Carbon nanomaterials with sp or/and sp hybridization in energy conversion and storage applications: A review. *Energy Storage Mater.* **2020**, *26*, 349–370. [[CrossRef](#)]



© 2020 by the authors. Licensee MDPI, Basel, Switzerland. This article is an open access article distributed under the terms and conditions of the Creative Commons Attribution (CC BY) license (<http://creativecommons.org/licenses/by/4.0/>).